Opto-Electronics Review

Review: Metamaterial/metasurface applications in antenna domain

Anitha C[1,3], Vivek Singh[*2,3], Ajay Kumar Dwivedi[2,3], Nagesh Kallollu Narayanaswamy[2,3]

[1] Department of Electronics and Communication Engineering, SJC Institute of Technology, Chickballapur, Karnataka, India
[2] Department of Electronics and Communication Engineering, Nagarjuna College of Engineering and Technology, Bengaluru, Karnataka, India
[3] Visveswaraya Technological University, Belgaum, India

Article info	Abstract
	Owing to their remarkable capability to modify electromagnetic waves at microwave and optical frequencies, metasurfaces are now the subject of a substantial amount of study and find utility in a wide variety of applications. These artificial sheet materials, which are typically made up of metallic patches or dielectric etchings in planar or multi-layer configurations with a thickness of subwavelength, have the benefits of being lightweight, easy to fabricate, and able to control wave propagation both on the surface and in the free space that surrounds it. This article provides an overview of recent advancements in the discipline and organizes those advancements according to their applications. The one-of-a-kind capabilities of many types of metasurfaces have come to light, beginning with the invention of frequency-selective surfaces, reconfigurable intelligent surfaces, and metamaterials. Patterning the metasurface unit cells allows for surface impedance to be altered and modified, which has wide-ranging applications in surface wave absorbers and surface waveguides. First and foremost, the purpose of this review article is to provide introductions to the fundamental metasurface, its important features, and application ideas. The authors address the most recent progress in metamaterial-inspired antennas and how they can be used to miniaturize antennas, increase gain and bandwidth, achieve circular polarization, and inhibit mutual coupling in multiple-input multiple-output (MIMO) antenna systems. In conclusion, exploring the research implications of the metasurface development trend and the significant engineering practical applications are shown in the conclusions.

1. Introduction

Currently, wireless systems are facing numerous challenges due to the rapid development going on in the field of communication systems, particularly in the area of antennas. The antenna plays an important role in radio engineering applications and wireless communication systems; hence it is important to give serious thought to antenna design and development. The modern communications system introduces multiple wireless standards and operational frequency bands all at once. Since IEEE 802.11 standards are used in mobile technologies from 2G to 5G, multiband antennas are intriguing. However, long-term evolution (LTE) advancements mandate smaller frequency operating ranges. Thus, it encourages the development of an innovative antenna design that operates over a wide bandwidth and can be integrated into any handheld device while maintaining the specified dimensions. These antennas are created using a variety of techniques and methods to create innovative structures, some of which are briefly detailed.

Microstrip antennas are typically employed because their TM_{01} and TM_{10} orthogonal modes enhance port isolation and minimize cross-polarization [1, 2]. An electric and magnetically coupled dipole antenna is used to increase bandwidth, achieve high gains, and improve radiation pattern [3]. Multiple printed circuit board (PCB) layers are used to extend bandwidth for multiband operation by exciting resonant modes on the plates [4, 5]. Antenna properties, including isolation, radiation pattern,

*Corresponding author at: vivek.10singh@gmail.com

and bandwidth, are improved by using parasitic components and various coupling strategies [6–8]. Antenna directivity, front-to-back ratio, and gain can be improved by resonant cavity antennas [9]. Lately, antenna researchers have paid a lot of attention to the metamaterial (MTM)-inspired antenna. Recent years have seen a paradigm shift in the study of the physical characteristics of electromagnetic (EM) components. MTMs development and their unique physical characteristics and novel engineering applications are mostly accountable for this inclination.

The introduction of MTM has considerably demonstrated new design techniques for materials, especially ones with unexpected properties compared to naturally occurring materials, as in Fig. 1 [10]. MTMs are considered to be artificial materials that have been manufactured and consist of unit cell structures that are periodic or non-periodic and have a diameter smaller than the wavelength of EM wave that passes through them [11]. An EM response produced by such a man-made array of unit cells can be precisely tailored by magnetic and electric wave components. As a result, a periodic arrangement of cell units can be thought of as an effective material with specifications for permittivity and permeability. It is agreed that this configuration will produce EM reactions at the necessary frequency, but that these responses will not manifest in naturally occurring materials. For instance, at microwave frequencies, magnetic materials are strongly bonded. However, metallic rings in array periodic structures show this magnetic response at high frequencies.

1.1   MTM development through history

The first artificial material exploration on a twisted chiral structural medium occurred in 1898 with Jagadis Chunder Bose's microwave experiment, which is when MTMs first came into existence [12]. Later in 1914, Lindman showed how chiral media affect EM waves by randomly arranging small helical-shaped wires within them [13]. Kock demonstrated the capacity to manipulate the refractive index of artificial media in 1948 by assembling metallic lattices in the shape of spherical discs [14]. Researchers working on artificial materials from all over the world have been motivated by the aforementioned ground-breaking works.

New ideas in the creation of composite materials from different geometrical configurations of the parts give rise to a new class of materials with exceptional EM properties that are not easily found in nature [15]. The electric and magnetic fields that develop within those customized materials, commonly referred to as MTMs, influence the two properties of the effective medium: permittivity and permeability. Specific EM properties of the MTM are largely defined by the physical organization, dimension, and alignment of the constituent materials. Veselago examined the concurrent negative permittivity and permeability of complex materials in a specific frequency range in 1968 [16]. For a sinusoidal plane wave in these artificial materials, he theoretically demonstrated the antiparallel direction of the Poynting vector and wave vector. Pendry showed in 1996 that it was possible to create artificial materials of negative permittivity in the GHz frequency range by periodic assembling of metallic wires to create a cubic lattice which is shown in Fig. 2 [17]. Three years afterward, Pendry and his colleagues suggested using a microstructure comprised of a split ring resonator (SRR) to tune the physical characteristics of the ring to produce a frequency-dispersive medium having negative permeability at various frequencies [18] (cf. Fig. 3). A 4×6 array of SRRs is shown in Fig. 3 to obtain a negative permeability structure.

In 2000 and 2001, combining SRRs and copper strips in the microwave regime allowed Smith *et al*. to experimentally demonstrate the existence of a composite media [19, 20]. By measuring the transmitted light scattering angle via a prism made of composite substances, the presence of a negative refraction index was confirmed. The SRR provides negative permeability because of the potent magnetic field between the rings, while the wire strips made of copper create negative permittivity over a particular frequency range. This gave a double negative material comprised of wire strips of copper and an SRR [20].
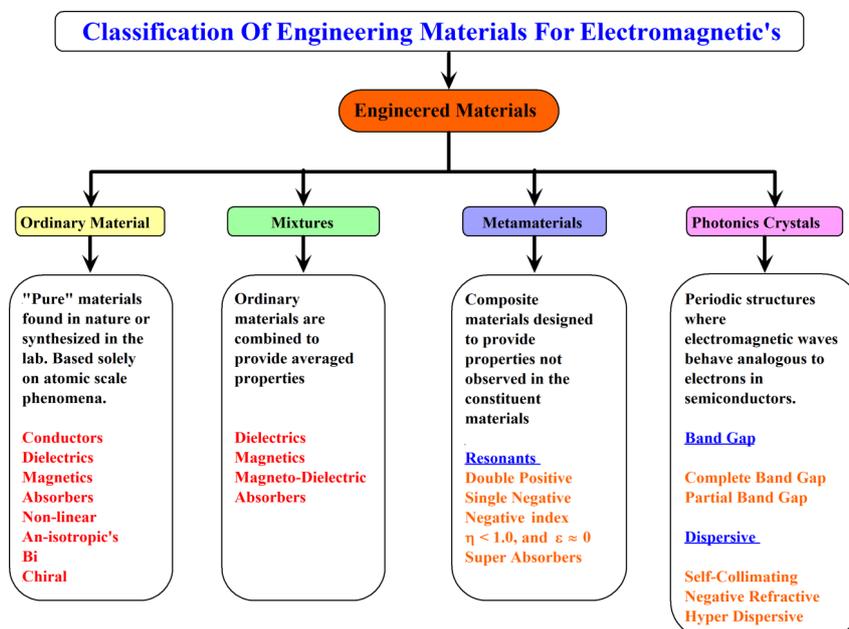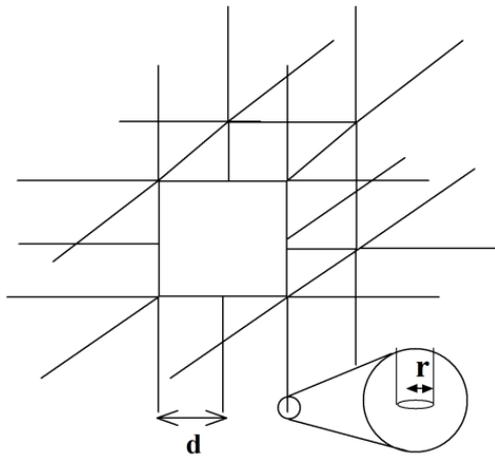

Fig. 1. Engineered material classification.

Fig. 2. Structural arrangement for achieving negative permittivity through wire strips.
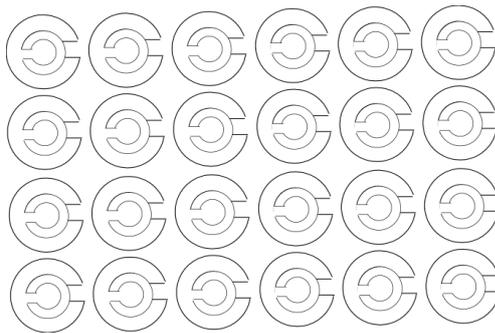

Fig. 3. Structural arrangement for achieving negative permeability through SRR.

1.2 Electromagnetic (EM) material classification

EM materials can be classified as natural materials and MTM by looking at the propagation constant β of the flowing current through the antenna [21]. If the β value is positive ($\beta > 0$), then the material is said to be natural. However, if β value is less than zero ($\beta < 0$) for a specific frequency range or zero at the nonzero frequency ($\beta = 0$), the material is categorized as MTM. EM materials can also be classified depending on the values of material permittivity ε and permeability μ as shown in Fig. 4 [22]. A medium with positive permittivity ($\varepsilon > 0$) and positive permeability ($\mu > 0$) is called a double positive (DPS), where the refractive index of the incident wave (n_i) is positive and that of the refracted wave (n_r) is also positive. Hence, the EM wave refracts normally with a positive angle of refraction (θ_r) for a DPS material. This field includes all dielectrics and water and it is shown in the first quadrant or top right quarter of Fig. 4; the materials are also called right-handed (RH) materials. A medium with negative permittivity ($\varepsilon < 0$) and positive permeability ($\mu > 0$) is called an epsilon negative (ENG) medium which is depicted in the top left quadrant of Fig. 4. In this medium, the wave does not propagate or undergo evanescent decaying. The medium in the bottom right quadrant is called μ-negative (MNG) as it is of negative permeability ($\mu < 0$) and positive permittivity ($\varepsilon > 0$). As in ENG, the wave does not propagate in this medium or undergoes evanescent decaying. In the bottom left quadrant, both
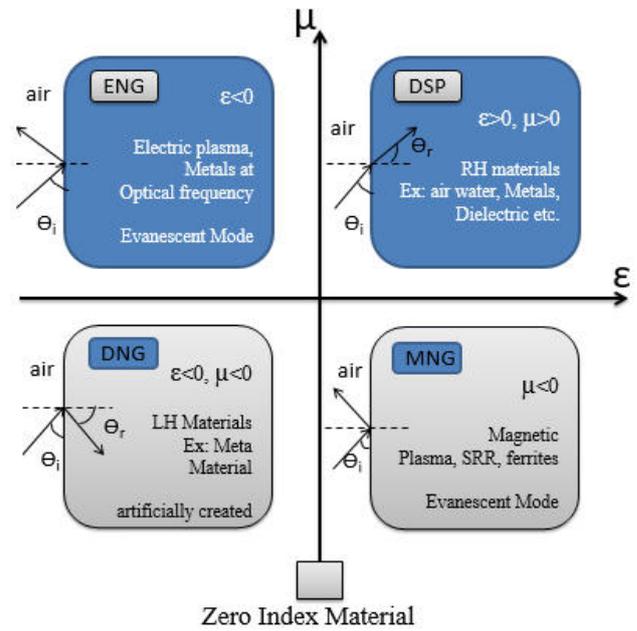

Fig. 4. Classifying the EM material based on permittivity (ε) and permeability (μ) (reproduced with permission [22]).
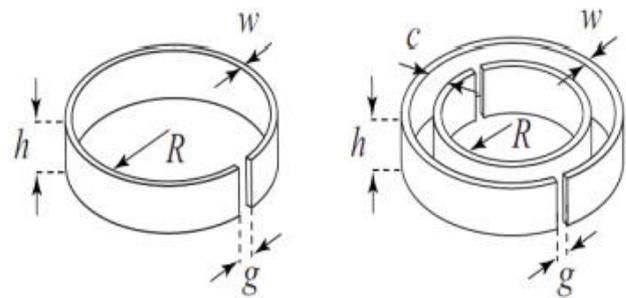

Fig. 5. SRR with a single ring (left), and double rings (right) (reproduced with permission [23]).

permittivity and permeability are negative ($\varepsilon < 0$, $\mu < 0$). Hence, the name is double negative (DNG) medium and the materials are referred to as left-handed (LH). Here, the EM wave gets refracted with a negative refraction angle $-\theta_r$. RH materials are naturally available, whereas ENG, MNG, and DNG are artificially created, which are often called MTMs.

One can come across various types of MTMs in general. Such as EM MTMs, terahertz MTMs, tunable MTMs, photonic MTMs, frequency selective surface MTMs, non-linear MTMs, and so on. SRR, also known as DNG MTMs, are widely used in multiple research areas as a part of terahertz MTMs, acoustic MTMs, and MTM antenna designs. SRRs are a pair of circumferential rings with splits at either end. The copper-coloured rings have a tiny gap between them and are constructed of a non-magnetic metal, as shown in Fig. 5. Each metallic ring has a circular gap that blocks the growth of current. The charges behave in a capacitance manner, gathering near the edge of the metal ring gap. An SRR functions as a resonant element when a capacitor and an inductor are present in a metal ring. Reference 23 contains the analytical equations for calculating effective capacitance and inductance.

1.3 Majorly used structures of MTMs

With MTMs, there is no restriction on how material properties can be designed other than by adhering to the basic physics rules. With the use of MTMs, it is possible to access the whole spectrum of material characteristics that mother nature permits and to precisely control those qualities. Due to this extraordinary degree of control, new materials have been demonstrated, including those with negative indexes, hyperbolic, or zero indexes, as well as transformational optical materials, which are utilized to create cloaks of invisibility along with other unusual structures. The MTM components of the microscopic level can be made out of any geometry or substance; designers can use their imagination and creativity to choose from an infinite number of design options to achieve the desired effects. The only requirement is that the spacing between the MTM elements must be smaller than the operating wavelengths. Some of the mostly used structures of MTMs can be seen in Fig. 6(a) [24] and Fig. 6(b) [25].

Many other artificial dielectric designs, such as very basic wires and "I-beam" structures like those in Fig. 6(b) that add segments to a wire top and bottom to raise the capacitance, might be seen as potential circuit MTMs. Raising the capacitance helps raise an artificial medium effective dielectric constant:

(a)

(b)

Fig. 6 Different MTM structures (reproduced with permission [24] and [25]).

$$\varepsilon_{\text{eff}} = 1 + \frac{l/d^2}{C},$$

where l is the length of the metal strip element to which an electric field is applied, d is the spacing between each element in a lattice structure, and C is the self-capacitance of the entire lattice structure. Materials typically exhibit magnetic response at extremely low frequencies, and they practically disappear near the wavelengths of visible light. SRR can create artificial magnetic fields when a variable magnetic field is applied to it. This responsive current travels in a loop, it creates a responding magnetic field. The unit cell structure of a loop with the split is called artificial magnetic MTMs. Resonant electric MTM components are referred to as electric inductive capacitive (ELC) and these are significant due to their ability to precisely alter a medium permittivity.

1.4 Metasurface (MS)

Metasurfaces (MSs) are optically thin subwavelength resonators that serve as dense two-dimensional (2D) analogues of engineered materials, or MTMs [26–28]. The constituent components unique characteristics, forms, type of mutual coupling, and strength, as well as the structure of the substrate, all influence the objects characteristics [29]. Due to their special capacity to modify EM waves in optical and microwave frequencies, MSs are a prominent research area and are employed in a variety of applications. They are extensively researched and used in EM fields due to their low weight and simplicity of production. From microwave to visible frequencies, MSs offer exceptional capabilities to block, absorb, concentrate, disperse, or guide waves on the surface, as well as in free space. High-fabrication losses and challenges, especially at the micro and nanoscales, limit the use of MTMs in many applications. However, MS sheets overcome the problems that the three dimensional (3D) MTMs encounter. Due to the benefits of increased quality, data rate, channel capacity, and reliability in scattering environments without requiring more transmitter power, MIMO systems are predicted to play a significant role in the introduction of 5G [30]. However, mutual coupling between spatial EM field and surface current on the substrate degrades the antenna radiation properties, which is one of the main issues for antenna designers. MSs are one of the methods used to reduce the mutual coupling between many antenna elements [31–34]. Many investigations of antenna designs using different MTMs and MSs have shown that these enhance the isolation between multiple input and multiple output antenna elements, increase bandwidth and gain, polarization conversion, and reduce antenna dimension.

1.5 Organization of the paper

This paper is divided into three sections. The first section includes an introduction, MTM development through history, major types and structures of MTMs, and a brief introduction to MS. Section 2 briefs about the applications of MS and MTM. Section 3 provides a detailed review of the design of the antenna using MTM and its achievements. Finally, section 4 concludes the paper.
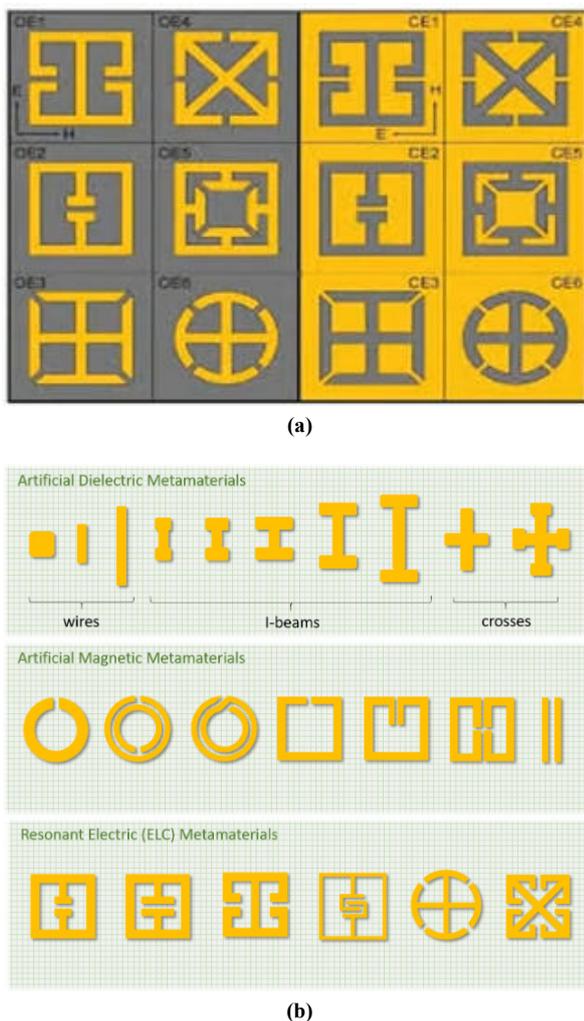
2. Areas of applications of MSs and MTMs

Researchers in the field of the EM theory have been inspired to build and create devices for a variety of applications as a result of the discovery of MTMs concerning propagation and radiation processes. Microwave network elements such as couplers [35–37], phase shifters [38, 39], absorbers [40], and filters [41] have found applications in MSs and MTMs. Other devices such as imaging systems [42], radars [43], satellites [44, 45], sensors [46], EM cloaks [40, 47], lenses [48, 49], seismic plots [50], and antenna applications, such as a new leaky-wave antenna (LWA)-based direction of arrival (DoA) estimate system are being introduced. Because of its effective electrical full-space scanning capacity, a composite right/left-handed (CRLH) LWA is used in this implementtation [51]. An LWA with a variable radiation angle, as well as beamwidth functions, is discussed and shown through an electronically regulated transmission-line construction based on MTMs [52]. Reference 53 presents a novel method of establishing an MTM EM bandgap (EMBG) arrangement in the pace between transmitting and receiving radiating elements in array antennas to reduce mutual coupling, thereby improving isolation. An MTM EMBG-inspired fractal isolator placed between radiating elements can also reduce mutual coupling [54]. An MTM-inspired LWA can scan from −25° to +40° which is based on slots and via-holes [55]. Reference 56 provides a thorough analysis of the fundamentals and practical applications of CRLH MTM LW and resonant antennas, emphasizing their special qualities and benefits over conventional antennas. In Ref. 57, novel antenna designs are presented that accomplish compact dimensions, wide-band operations, and multiband capability by utilizing the special qualities of MTMs. For a millimetre-wave application, Reference 58 describes the design of CRLH-LWA which offers an effective approach for modern systems of communication. The principal objective in Ref. 59 is to design and characterise a new CRLH unit cell that capitalizes on the special qualities of MTMs for use in cutting-edge antenna applications.

LWA in dominant mode, that can scan its beam from backfire-to-endfire based on CRLH transmission lines is successfully shown in Ref. 60. Reference 61 looks into adding MS walls to a dielectric resonator antenna (DRA) in order to increase its gain. Through the utilization of MTMs special qualities, Reference 62 demonstrates that it is feasible to greatly improve the bandwidth and radiation efficiency of electrically small antennas. The antenna creative use of MTM components in Ref. 63 allows it to achieve circular polarization (CP) and multi-band operation, resulting in a good performance over the whole required frequency range study. Reference 64 effectively shows that an MTM superstrate concentrates emitted energy and can increase gain without adversely compromising the efficiency or bandwidth of the antenna. A compact, effective antenna with exceptional performance characteristics is produced in Ref. 65 by combining CRLH-MTM with a substrate integrated waveguide (SIW) technology. This makes the antenna appropriate for high-end applications that require dynamic beam-steering and good isolation.

Additionally, the MTMs discipline conducts research in acoustics, materials science, and thermodynamics [66–67]. In this paper, prominence is given to planar antenna design using different types of MTMs and MSs . Different techniques to incorporate MTMs in the structure of patch antennae with MIMO configurations are also discussed.

3. MTM/MS applications in antenna engineering

One of the most crucial components of wireless communication is antenna engineering and artificially designed materials have become prevalent in this area because of their amazing capacity to adjust the intensity, phase, and polarisation of EM waves [68]. This section has been divided into subsections for bandwidth improvement, gain optimization, and miniaturization of microstrip patch antenna using the MTMs and the MSs which are loaded on to the patch, or positioned at the ground plane, integrated into the substrate, or mounted above the main radiator in order to keep this work precise.

3.1 Bandwidth and gain improvement

Wide bandwidth and high gain are now more important than ever in wireless communication. However, due to weak radiation characteristics, the performance of small low-profile antennas suffers in terms of gain and efficiency [69–72]. The literature offers a variety of methods for boosting an antenna gain and bandwidth, including the use of parasitic elements, customized ground planes, and more [73–77]. Whilst these methods boost radiation properties, they do so at the expense of added complexity. This is where adding MTM with a unique resonator structure has a significant impact on reducing complexity and enhancing antenna characteristics.

3.1.1 MTM/MS loading on the main resonator

MTM structure placed close to an antenna directs EM radiation in a particular direction, increasing the antenna gain. Figure 7(a) depicts an antenna structure loaded with modified Jerusalem crosses and a square-shaped MTM surface that resembles a checkerboard [68]. As demonstrated in Fig. 7(b), by rotating the Jerusalem cross-shaped unit cell placed at the patch antenna top and bottom radiating edges by 45 degrees, a gain improvement of 3.6 dB peak was achieved.

For a WLAN application, a partly grounded antenna patch with a modified U-moulded link was created which resonates from 2.4–2.484 GHz and from 8.01–8.5 GHz with higher gain and bandwidth without changing the antenna radiation properties [78]. Three U-shaped transmission links and an altered ground plane are used to create the antenna two unique resonant modes. Utilizing an improved loading process, a regular recurring arrangement of MTM cell units incorporated over the same surface of the substrate has increased the antenna performances. The bandwidth of the designed antenna increases by 16% and 6% in upper- and lower-frequency bands, respectively. Also, the gain was improved by 3.63 dB for 2.63 GHz and 1 dB for 8.45 GHz which is shown in Fig. 8.
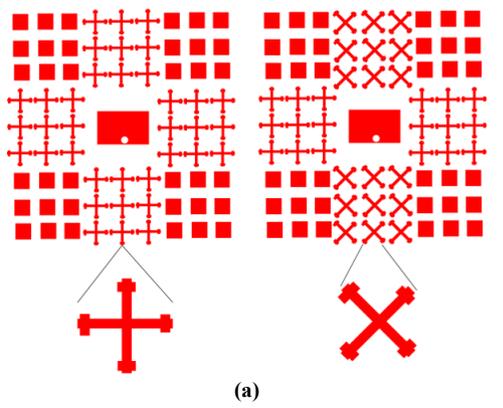
(a)
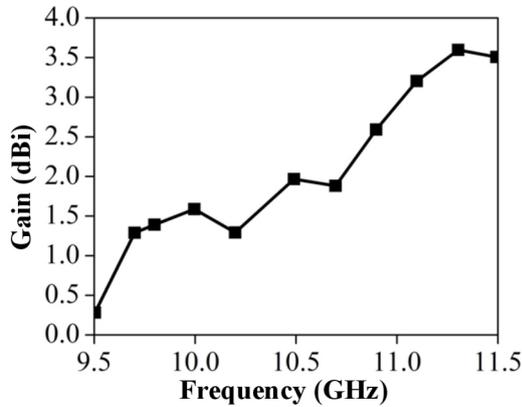
(b)

Fig. 7. (a) Artificial magnetic conductor material-loaded antenna structure. (b) Gain enhancement plot.
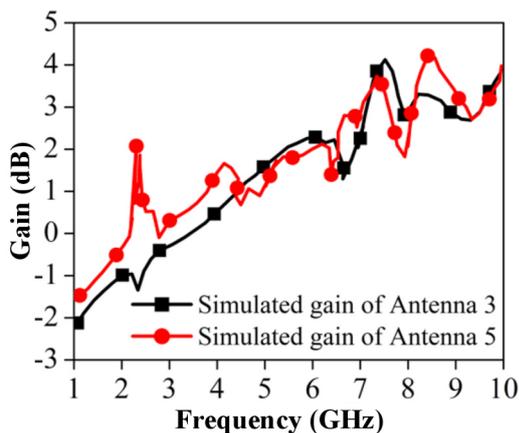

Fig. 8. Gain plot of the fabricated antenna.

In Ref. 79, a patch antenna truncated corner has been surrounded by a series of tailored SRRs that are diagonally resonating between 2.4–2.484 GHz lower band and 5.15–5.85 GHz upper band. The positioning of the MTM is planar to the primary radiator, which reduces the complexity of the design and increases the lower band gain by 3.69 dB. Figure 9 depicts the gain plot of a fork-shaped conformal antenna that resonates between 3.1 and 3.88 GHz in Ref. 80 and is loaded by a 3 × 6 array of dual S-shaped unit cells with low MTM refractive index design and parasitic elements in the shape of triangles which give a gain enhancement of 1.8 dBi (decibels isotropic) for the complete operating frequency range compared to that of a basic antenna.
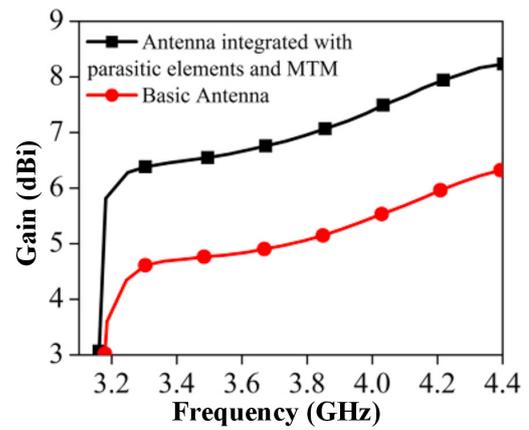

Fig. 9. Gain plot of the basic and conformal antenna.

Two flower-shaped DNG MTM lens layers are placed at an appropriate distance from the microstrip patch antenna. The lens layers are kept 5 mm apart, and the first lens layer is kept 10 mm from the patch. This construction improves the antenna gain by 71% and directivity by 50% compared to an antenna without MTM layers [81]. Figure 10 shows the gain plot of the flower-shaped MTM structure-inspired antenna.
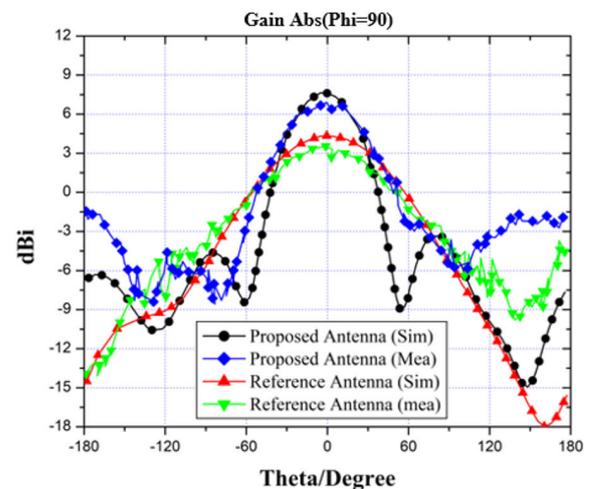

Fig. 10. Gain plot of the flower-shaped DNG MTM antenna.

In Ref. 82, a radiating dipole is surrounded by a DNG shell, which increases the amount of power radiated and, hence, the gain. It has been shown that by properly adjusting the inner radius of the DNG shell and by further making the DNG shell more negative, the radiated power gain can be enhanced.

Reference 83 proposes a wideband MIMO antenna design for a 5G sub 6 GHz system. The antenna has four patches, which are cut at the diagonals by a square, as shown in Fig. 11(a). The four-patch antenna uses Roders RT5880 material as substrate. It has an MS sheet of a 10 × 10 array of MTM unit cells with a copper-coated backplane at the rear side with an air gap of 12 mm from the MIMO antenna. This gap is required for enhancing the gain of the antenna as it allows the desirable interference between radiation and reflected signal from the MS . This construction achieves an 8.3 dBi maximum gain, 82% total efficiency, and a wide bandwidth from 3.08 to 7.75 GHz. However, the antenna gives 6.8 dBi and 7.5 dBi gain for
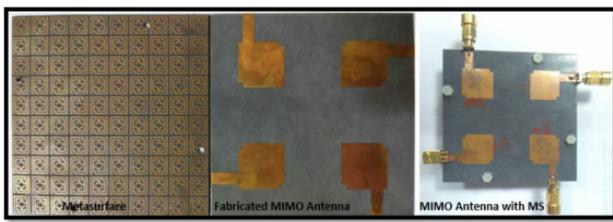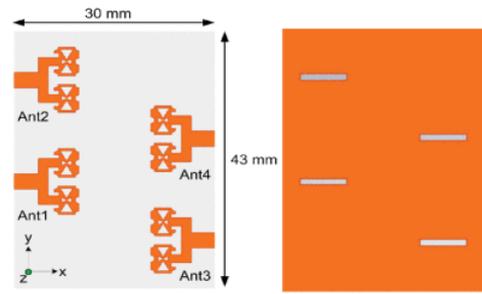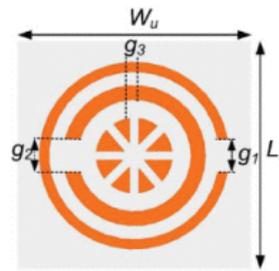
(a)
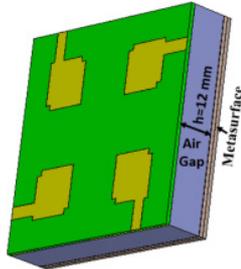
(b)
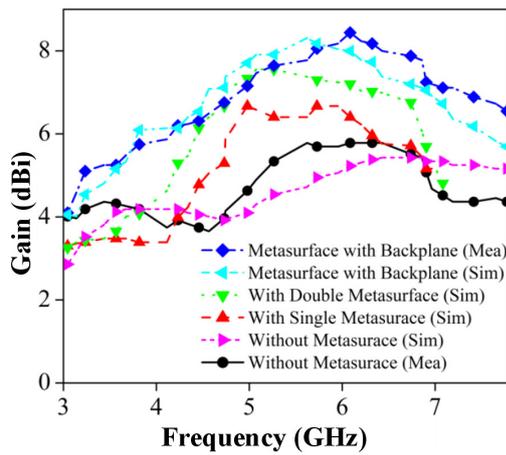
(c)

Fig. 11. Antenna design using MS as a backplane: (a) 10×10 MS array in the rear side and fabricated MIMO antenna, (b) simulated MIMO antenna with MS, (c) gain plot of simulated and measured results (reproduced with permission [[83]]).

(a)

(b)

(c)

(d)

Fig. 12. (a) MIMO antenna top and bottom view. (b) MS cell unit. (c) Gain plot. (d) Fabricated MIMO antenna (reproduced with permission [84]).
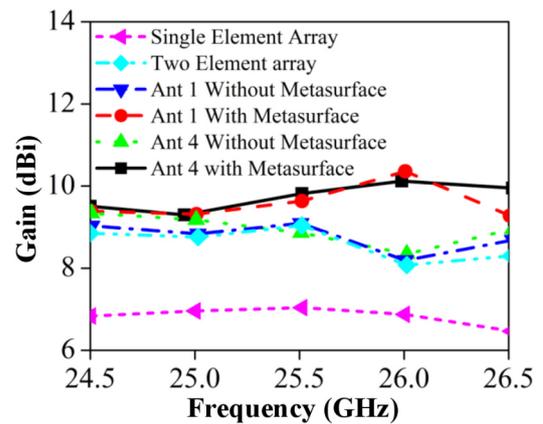
single-layer and double-layer MS sheets, respectively. Hence, it can be seen that a copper-coated backplane MS sheet gives more gain compared to single- or double-layered sheets. The gain plot of with and without MS, single- and double-layered, and MS with a copper-coated backplane is given in Fig. 11(c). In support of millimetre-wave 5G applications, a four-element MIMO antenna with a one-layered MS is proposed for an operating bandwidth from 24.55 to 26.5 GHz [84]. Each MIMO component consists of an aligned feeding circuit and a 1×2 array antenna as in Fig. 12(a). The MS is made up of a nine- by a six-unit cell array, each of which is a resonator in the shape of a circular split ring (CSR). This arrangement achieves a maximum gain of 10.27 dBi as given in Fig. 12(c). The MS sheet is placed at the top of the antenna system through a gap of 0.5 λ which is shown in Fig. 12(d). With a peak gain of 9.18 dBi, a patch antenna described in Ref. 85 uses irregular patches of the MS, stair-shaped openings, and parallel waveguide feeding. Each subwavelength patch acts like a radiating component, and when combined, they have the effect of a radiating plane

array, increasing the gain of an antenna. By enhancing the coupling that exists between the MS and the aperture located at the top and bottom of the substrate, the suggested antenna bandwidth is increased.

In Ref. 86, it is suggested to use high-frequency impedance to increase the monopole antenna gain. Surface waves are reduced by high impedance surface (HIS), which also aligns incident waves and reflected waves in phase. HIS at the resonant frequency is caused by the presence of a weak magnetic field over the surface. In comparison to an antenna with no HIS, the created fork-shaped monopole attains a bandwidth of 32.3%, as well as a gain of 4.5 dBi.

Reference 87 describes a Fabry–Pérot antenna that has been covered with a superstrate coating made of a revised Jerusalem cross and close ring cell units of 2D MTM organized in a checkerboard pattern to enhance both the radiating and transmitting performances. The primary antenna geometry, along with the top and bottom surfaces, is structured like a chessboard. The wideband frequency between 9.4 and 11.2 GHz has undergone a 4.9 dB gain boost. In Ref. 88, a bowtie dipole MIMO antenna patch is suggested that utilizes artificial magnetic conductor (AMC) loading for significant gain and bandwidth. Here, the bowtie antenna is combined with V-shape parasitic patches to provide two resonant modes. Instead of using a perfect electric conductor (PEC) ground plane, an AMC ground plane is positioned below the patch of radiation at a distance of 10.5 mm to increase gain. A high gain of 7.1 dBi, bandwidth of 31% (3.0–4.1 GHz), and terminal isolation of more than 25 dB were all recorded for the proposed design.

3.1.2   MTM/MS-inspired antenna

By etching the unit cell structures into the radiating patch, ground plane, or in between a ground plane and a patch, an MTM-inspired antenna can be created. The number of unit cells can be one or more, and when they combine with the antenna, they exhibit characteristics like negative permittivity (medium ENG), negative permeability (medium MNG), and both negative permittivity and permeability, which do not exist in nature. SRR, complementary SRR, strips with SSR, and complementary split ring resonator (CSRR) are the most popular types of structures, along with artificial magnetic conductors.

A proposed microstrip patch antenna has a ground plane loaded with CSRR [89]. The patch exhibits an excellent gain of 5.93 dBi at resonance, a slightly higher bandwidth, and a 10% reduction in size when compared to an antenna without loading by adding CSRR to the ground plane. The ground plane CSRR slots alter the microstrip antenna resonant properties, causing it to resonate at a low resonant frequency. The antenna gain plot is shown in Fig. 13. One of the potential MTMs, an AMC, is used to increase the gain of microstrip antennas. At resonant frequencies of 3.6 GHz, 5.86 GHz, and 8.53 GHz, respectively, an increase in gain of 4.95 dBi, 3.88 dBi, and 4.13 dBi was achieved by applying an artificial magnetic conductor beneath the substrate of a coplanar waveguide fed microstrip antenna [90] which is shown in Fig. 14 and Fig. 15.
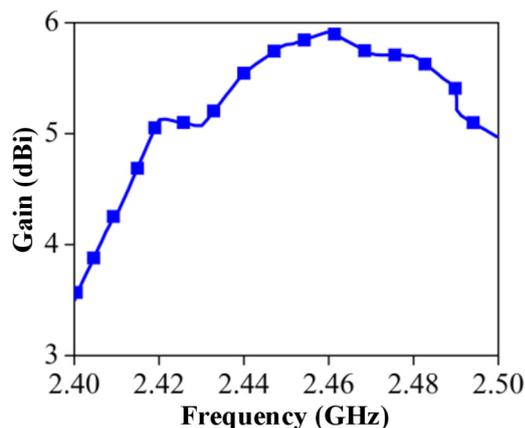

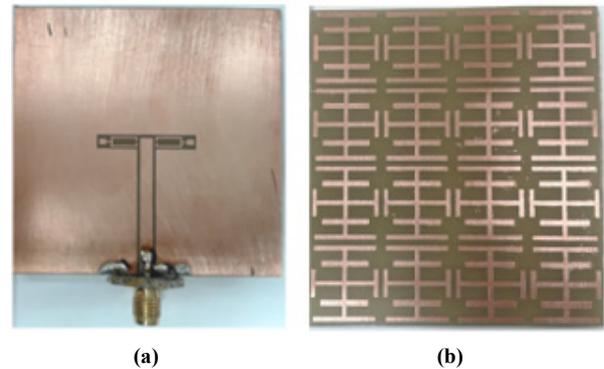**Fig. 13.** Gain plot of the CSRR etched antenna structure.

(a)   (b)

Fig. 14. AMC loaded triple-band slot-patch antenna. (a) Top view, (b) bottom view.
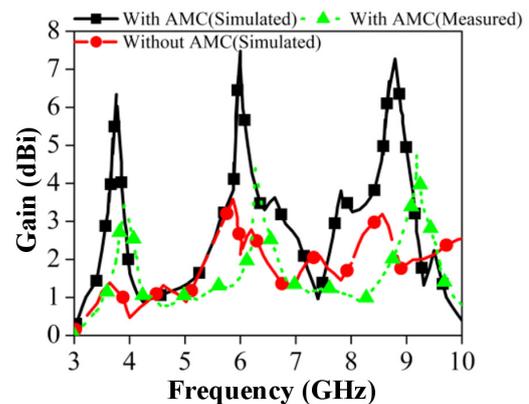

Fig. 15. Gain plot of the AMC loaded triple-band slot-patch antenna. (Reproduced with permission [90]).

In Ref. 91, many corrugated, non-corrugated SRR MTMs are placed onto microstrip-based radiating structures. Corrugated structure means the square teeth were added onto the SRR. Gain and bandwidth are increased by changing the distance between the rings, the highest gain of 7 dB is obtained for two corrugated SRRs, and the highest bandwidth of 420 MHz is obtained for three corrugated SRRs. This reference paper shows the antenna parameters measurements for eight different types of SRRs to be loaded onto the radiating patch. Measurements show that there is a good increase in the gain and bandwidth with small gaps between the rings in SRR as compared to the large gaps.

3.1.3   MTM/MS integrated substrate

Due to a surface wave excitation, the radiation efficiency and, consequently, the gain decrease when a microstrip antenna is reduced in size using a high permittivity substrate [92]. Researchers have employed MTMs within the substrate to lessen this issue. In Ref. 93, a decent gain of 5.93 dBi at a resonant frequency, a little bit greater bandwidth, and a 10% size reduction over the unloaded antenna are all achieved by adding CSRR to the patch ground plane. Utilizing SRR structures, which stimulate and combine two resonant modes, the microstrip antenna bandwidth is increased. Figure 16 depicts the return loss of the MTM-loaded antenna. A μ-negative array of 3D SRRs is implanted within a low-temperature cofired ceramics substrate material of the coaxial probe-fed patch antenna that resonates at 5.2 GHz [94]. There is a bandgap of about
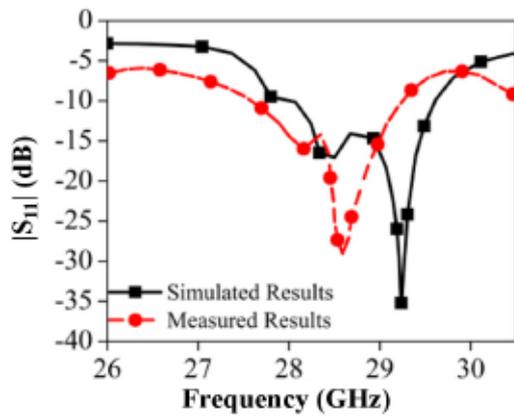
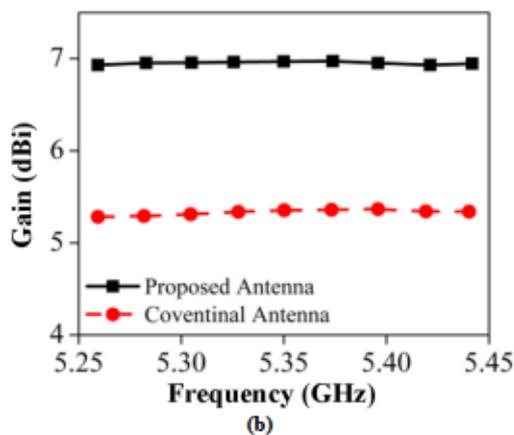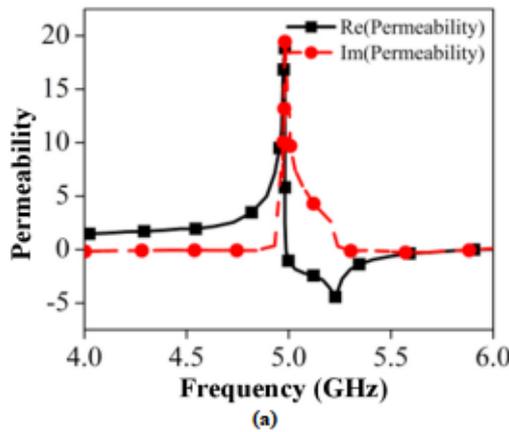**Fig. 16.** Return loss of antenna with MTM substrate integration [93].

Fig. 17. Antenna design using MTM integrated substrate: (a) permeability of unit cell, (b) gain plot.

Fig. 18. Antenna with EBG to increase gain and bandwidth: (a) reflection coefficient, (b) gain/efficiency plots.

Y-shaped construction as a radiator and is partially ground incorporated with EBG, has a broad bandwidth of 3.1 to 10.6 GHz, a maximal gain of 6.25 dBi, and excellent radiation qualities. Band stop response grows as the fork slot linked capacitance increases as its size does.

The related work in gain and bandwidth enhancement is summarized in Table 1.

3.2 Linear polarization (LP) to circular polarization (CP) conversion

Antennae are transducers that convert electrical signals into EM waves and radiate into space. Polarization of these signals is of utmost importance for any application. A system mainly communicates in either LP or CP. EM wave electric field is constrained to one axis along its propagation direction which is named LP, so the electric field is either perpendicular or parallel to the surface. LP is classified as horizontal polarization, vertical polarization, and slant polarization. CP is one in which an EM wave electric field is made up of two field components of equal magnitude, but $\pi/2$ phase difference and the EM wave rotates along the propagation direction, so radiation is achieved in all directions. If rotation takes place clockwise, then it is called right-hand CP (RHCP), anticlockwise rotation is referred to as left-hand CP (LHCP). CP waves are more reliable, have a longer range, and are less susceptible to bad weather and obstructions than LP waves. CP antennas outperform conventional linear technologies

5.2 GHz where EM waves become reflected, as can be seen from the obtained permeability values of the MTM cell unit in Fig. 17(a), and this insertion in substrate increased the gain of the antenna by 1.5 dB.

In order to stop or facilitate EM wave propagation for all the incident angles over a specific frequency band, EM bandgap (EBG) devices are typically constructed as periodic/non-periodic arrangements of unit cells. EBG acts as a transmitting or reflecting surface, resulting in a low profile, reduction of the surface waves, and excellent gain in antenna design [95]. In Ref. 96, a square patch is used to create an EBG structure utilizing a configuration of cross-shaped and fork-shaped slots. The suggested monopole antenna, which is seen in Fig. 18 and has a serrated
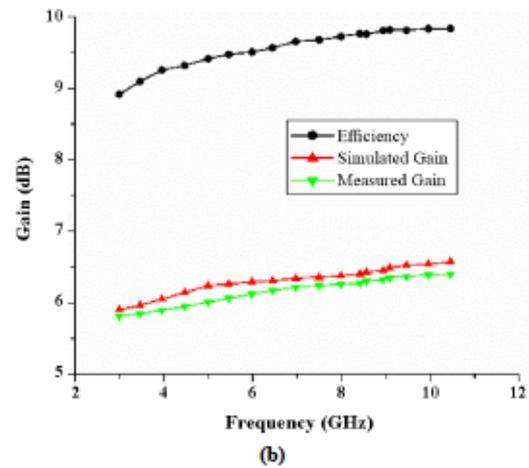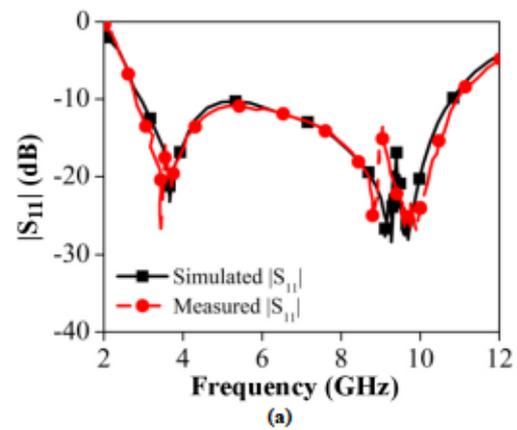
Table 1.
Related work in gain and bandwidth enhancement.

Ref.	Antenna + MTM type	Gain (in dB)	Bandwidth enhancement (in %)
[97]	Loop antenna + MNG cell unit	4.8	52
[98]	Patch antenna + SRR and wire strips superstrate	12.1	89
[99]	Wideband cavity antenna + superstrate as a partly reflecting surface	13.78	15.5
[100]	Slot antenna + EBG	5.93	18
[101]	Endfire antenna + U-shaped reflector	6.8	62.6
[102]	Fabry–Pérot cavity + superstrate with ring shapes on upper side	11.2	22.2
[103]	Zeroth order resonant (ZOR) antenna + AMC reflector	7.1	89
[104]	Wideband antenna CRLH structure transmission line (TL) – CRLH-TL	6	139.19
[105]	ZOR antenna + CRLH	3.75	71.11

in many ways thanks to these cutting-edge signal propagation features. Thus, CP antennas provide superior connectivity with both stationary and mobile devices since their CP radiation eliminates alignment problems. Additionally, they are better at signal strength via obstacle and penetration. An axial ratio (AR) is an essential fundamental parameter for evaluating antenna CP. In practice, the AR should be less than 3 dB but is required to be 0 dB for a perfect CP. The AR represents the ratio of CP axis to the minor axis [106]. In literature, various methods for achieving CP are described, patch disrupting [107, 108], rearranging feed [109], and loop antenna usage [110] are some of those. This section describes how MTM is used for achieving CP.

3.2.1   MTM/MS loading on the main resonator

Strong CP features in the operational bandwidth will be provided by the loading of various MTM/MS structures in conjunction with the antenna. MS is the most effective way for the conversion of LP to CP of EM waves, as well as enhancing other antenna characteristics including bandwidth, gain, and miniaturization. In Ref. 111, a chiral MTM polarizer-equipped CP microstrip patch antenna is proposed to be designed at an operating frequency of 2.4 GHz. The design of the CP antenna is done in two phases, the first two triangles of the same length are made on a rectangular patch. To produce CP waves, the triangular slots offer a perturbation that produces two perpendicular surface current signals with a phase shift of 90°. Second, the chiral MTM structures are used to operate like polarizers, allowing just the dominant CP wave to pass through while filtering out the weaker wave. The addition of chiral components in the antenna design gives an increased gain of 6.91 dBi and an AR of < 3 dB as shown in Fig. 19(a) and (b). An antenna with adjustable polarization and high gain is presented in Ref. 112 which operates at a frequency of 2.8 GHz. It consists of three layers, with the top layer being a μ-negative MTM (MNM) and acts as a partially reflecting surface (PRS), which is made up of an array of patches and crosses on either side of a dielectric material. The middle layer is an air-filled cavity, with the lower layer having a radiating patch on the upper side and a ground plane on the lower side of the substrate, as in Fig. 20(a). An LP EM signal gets converted into a CP EM wave utilizing this microstructure as shown in Fig. 20(b). The antenna gives 1.02 ARs at 2.8 GHz and a better gain of 13.70 dBi
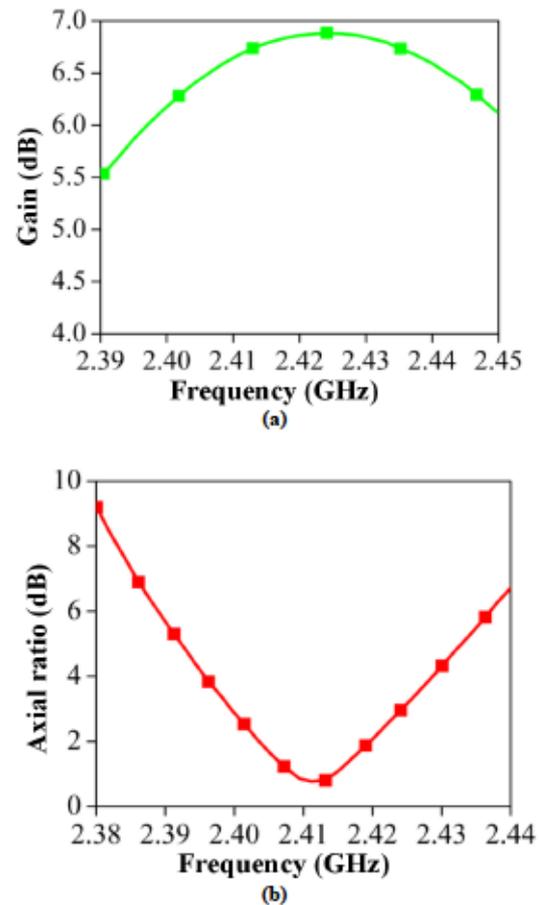
Fig. 19. Microstrip antenna based on chiral MTM: (a) gain plot, (b) AR plot.

for LHCP. By rotating the top layer by □/2, the antenna becomes an RHCP, which also gives good AR gain values. Figure 20(c) and (d) shows fabricated antenna and plot of AR.

The massive capacitively-loaded loop (CLL) near-field resonant parasitic (NFRP) elements in the electric monopole antenna system produce the appropriate CP. In Ref. 113, CP antennae with two monopole CLLs are placed vertically perpendicular to each other on a common ground plane, which act as NFRP elements. This configuration gives an AR of less than 3 dB for over a band of 1.3590 to 1.4169 GHz and a gain between 5.81 and 5.93 dB. A similar design is used in Ref. 114, where single-band and

(a)

(b)

(c)

(d)

Fig. 20. MTM-loaded planar CP antenna (reproduced with permission [112]). (a) 3D antenna schematic structure, (b) CP behaviour (c), LHCP antenna photograph, (d) AR plot.

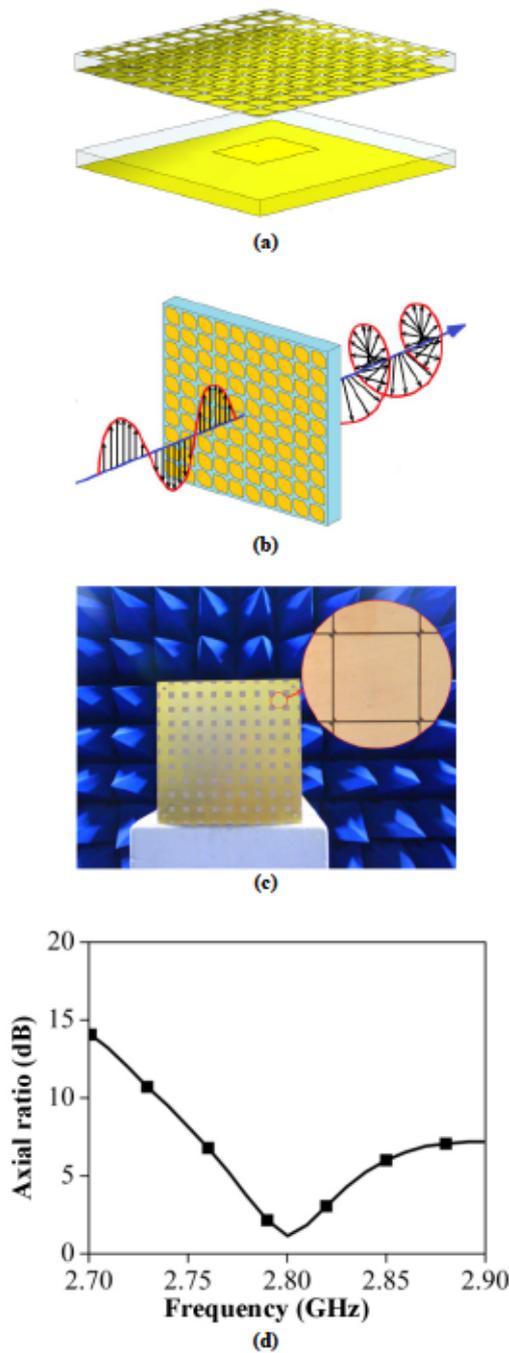dual-band protractor CP antennae are presented. The AR is around 0.44 over a bandwidth of 7.4 MHz for the GPS L1 band. The dual-band antenna gives AR = 0.87 over a band of 5.3 MHZ and a gain of 6.2 dB for GPS L1 resonant frequencies whereas AR = 0.42 for a bandwidth of 4.3 MHz and a gain of 5.36 dB for GPS L2 band.

In Ref. 115, two rings are connected diagonally with a strip to form a single cell. Such 16 cells are arranged in a 4 × 4 format with each cell of a 20 × 22 mm² dimension to complete the MS structure. This structure can divide an incident waveform into two perpendicular components with identical amplitudes and a □/2 phase difference. Four different radiating elements are designed which are micro-

strip feed, coaxial feed, slot, and aperture antenna. The MS layer was used as a superstrate and provided better results when tested on all four types of antennas designed. Aperture antenna with MS achieved an impedance bandwidth of 710 MHz from 2.16 to 2.87 GHz, AR bandwidth of 80 MHz from 2.56 to 2.64, and a maximum gain of 7.8 dB. The same was measured by fabricating the aperture antenna as given in Fig. 21(a) and (b).
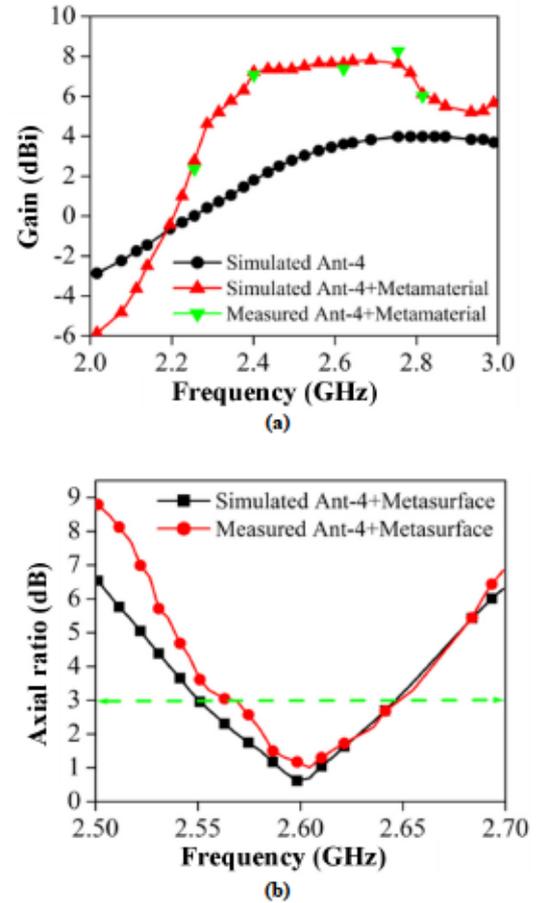

(a)

(b)

Fig. 21. Novel MS for polarization conversion: (a) gain plot after insertion of MS, (b) AR plot.

In Ref. 116, MS cells are designed for RHCP and LHCP signals. A patch and a slot are used as simple antennae to produce an LP signal which will be converted into a CP signal with the help of the MS layer used as superstrate. Four antennae were designed, LH MS on patch antenna gives MS antenna 1, RH MS on patch is MS antenna 2, LH MS on the slot is antenna 3, and RH MS on the slot is antenna 4. Figure 22(a) and (b) show the AR bandwidth (AR < 3 dB) of antenna 1 and 2, respectively.

3.2.2   MTM/MS-inspired antenna

An CP antenna is typically influenced by its configuration and the components that are mounted on it. To achieve the CP behaviour of an antenna, the SRR and CSRR MTM elements are also utilized. The CP antenna design for applications in satellites based on SRR and CSRR MTM components was presented in Ref. 63. It has a radiating stub on the other side of the feedline and a defective ground construction. The intended antenna has a max gain of 4.8 dB and at frequencies of 2.39 to 2.55 GHz, 3.05 to 3.1 GHz, 4–5 GHz, and 6.3 to 6.64 GHz,
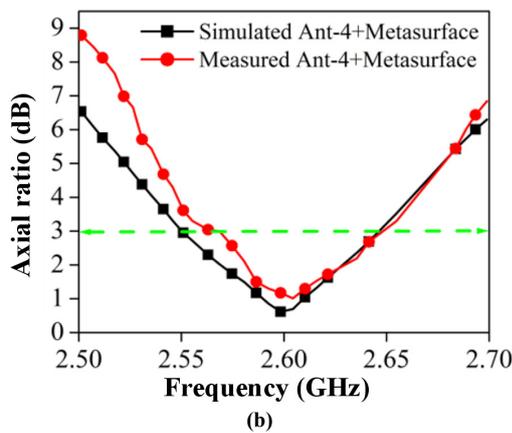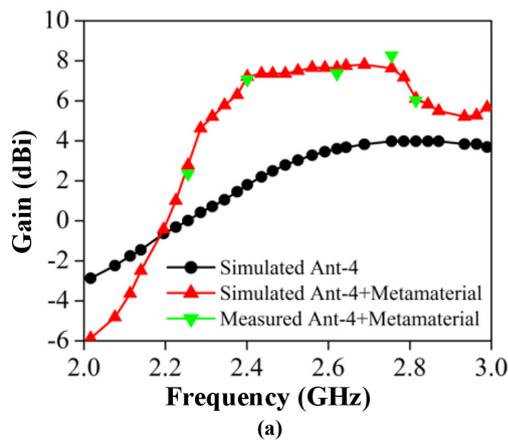
Fig. 22. (a) AR plot for MS antenna 1, (b) AR plot for MS antenna 2.

Fig. 23. Quad-band CP antenna: (a) reflection coefficient plot, (b) AR plot for different frequencies.

respectively, it displays CP as shown in Fig. 23(b). In Ref. 117, the developed antenna for implantable applications has two split ring resonators and operates between 2.4 and 2.5 GHz in the industrial sector, science, and medical spectrum. The FR4 substrate was used in the construction of the implantable antenna and it offers a superior gain of 4.86 dB, a smaller size dimension of 29×28 mm^2 (84% size reduction), good impedance matching, CP, and 3 dB AR bandwidth of 3.41%. The antenna AR plot is given in Fig. 24. A square-shaped microstrip patch antenna with two diagonally opposed corners is clipped, and the ground plane is then loaded with the proposed split-circular MTM ring array [118]. The gain and bandwidth of the conventional patch antenna, which has mitered corners and 2.4 GHz resonant frequency, are 4.8 dBic and 500 MHz, respectively. But when split-circular MTM rings are loaded onto the ground plane, the gain is enhanced by 0.4 dBic, and bandwidth is increased by 15 MHz. This structure 3 dB AR bandwidth is 610 MHz. The suggested microstrip patch antenna has an overall dimension of 37.53 mm $\times$ 37.53 mm $\times$ 1.6 mm.

3.2.3   MTM/MS-integrated substrate

Reference 119 outlines the design and fabrication process of a monopole antenna with dual-band and dual-polarization capabilities. The antenna is constructed using MTMs and is intended for use in wireless applications. Unit cells with dimensions of 1.6 mm $\times$ 17 mm $\times$ 24 mm were prepared and exhibit resonance frequencies of 3.5 GHz and

Fig. 24. AR plot of implantable antenna.

5.5 GHz. The antenna exhibits LP in the first frequency range and CP with an AR bandwidth of 150 MHz in the second frequency range. It provides a gain of 4 dBi in the first frequency range and 5.1 dBi in the second frequency range. Figure 25 depicts a fabricated antenna and its accompanying AR plot.

The major reason for the LP to CP conversion is identified by an extensive theoretical investigation, as described in Ref. 120. Figure 26(a) and (b) shows a circular pie-shaped single MS layer with a rectangular patch at the origin, which is retained on a polytetrafluoroethylene (PTFE) substrate with a dielectric constant of 2 and a thickness of h = 1.6 mm. The length and breadth L, W of the patch, as well as the radius r_0 of the MS cell, are

optimized to produce better outcomes. Figure 26(c) shows that this setup achieves 98% efficiency over 20–34 GHz and an AR bandwidth (AR < 3dB) across the 20.18–33.93 GHz band. It also transforms the LP signal to the RHCP signal.

Summary of work on LC to CP conversion is shown in Table 2.

3.3 Isolation enhancement

A growing number of high data rate technologies, notably 5G and 6Gk, as well as additional wireless and mobile technologies, are using MIMO to achieve higher levels of efficiency. MIMO basically uses many antennae on the transmitter side and the receiver side to take advantage of the multipath phenomena that are always there and transmit additional data rather than producing interference. Further, there are certain merits to using MIMO technology, such as increased non-line-of-sight (NLOS) and quasi-NLOS connectivity, better signal span, decreased bit errors, reduced power consumption, and less interference. However, there are a few demerits of MIMO
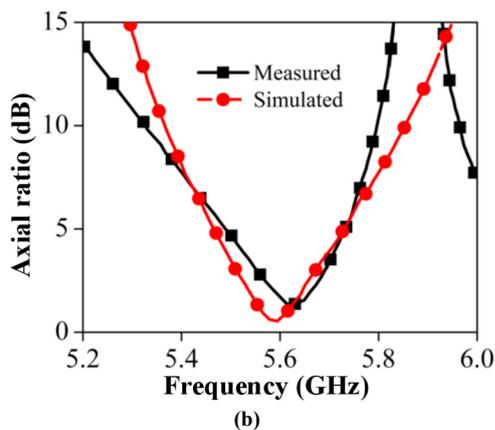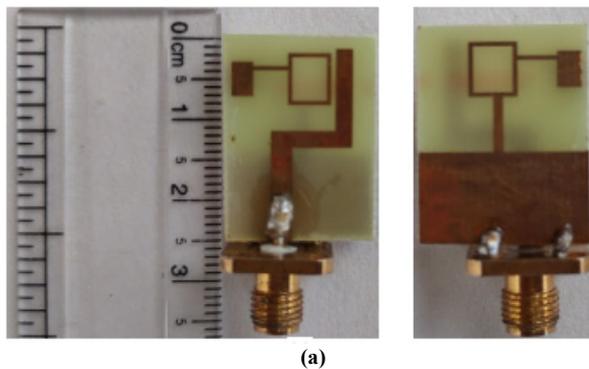
Fig. 25. CRLH MTM-inspired antenna (reproduced with permission [119]). (a) Fabricated top and bottom view, (b) AR plot.
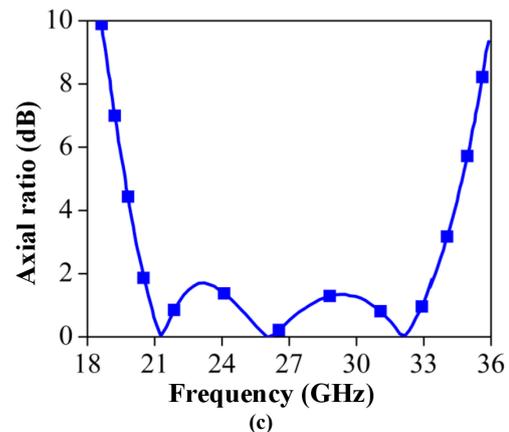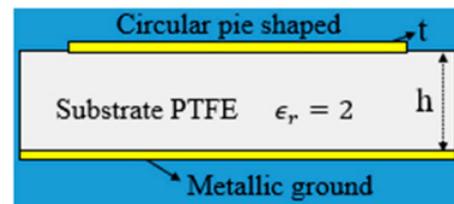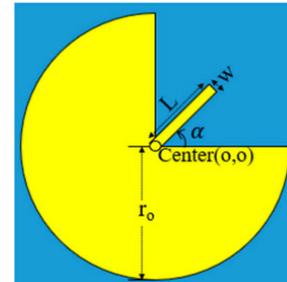
Fig. 26. An ultrawide band MS antenna (reproduced with permission [120]). (a) Top view of MS with patch, (b) side view of design, (c) AR plot.

Table 2.
Summary of work on LC to CP conversion.

Ref.	Antenna type + MTM	Gain (dB)	ARBW
[111]	Microstrip patch + chiral structures	6.9	25 MHz
[112]	Square patch + MNG	13.7	AR = 1.02 at 2.8 GHz
[113]	CLL-NFRP	5.81 to 5.93	57.9 MHz
[114]	Dual-band protractor	5.36	4.3 MHz
[115]	Aperture + MS	7.8	80 MHz
[118]	Microstrip patch + circular split MTM	4.8	610 MHz
[119]	Dual-polarized monopole + CRLH	5.1	150 MHz
[121]	Microstrip planar antenna array + MS		210 MHz
[122]	Microstrip line-fed elliptical antenna + MS	7.5	350 MHz
[123]	Slot + MS		1.1 GHz

antennae. Along with comparatively high cost due to the usage of multiple antennae, mutual coupling between the antenna elements is the most talked about. The EM reaction among antenna components in an array is known as mutual coupling. Each antenna component within the array develops current based on its own excitation, as well as contributions from nearby antenna elements. The term "mutual coupling" refers to the energy that a neighbouring antenna absorbs when another antenna is active. The input impedance, reflected coefficients, and patterns of radiation of the array elements are typically altered by mutual coupling [124]. To have a smaller form factor, the MIMO antenna needs to be highly compact. When several antennae are mounted on a single substrate, the compactness of the MIMO antenna is a major challenge. The antenna will suffer from surface wave and space wave coupling effects if the spacing between antenna components is less than $\lambda_0/2$, or half of the free space wavelength. Given the substantial losses of power in rich scattering surroundings, the performance of MIMO antennae degrades as compactness increases due to an increase in the likelihood of mutual coupling effect. As a result, the structure of a compact MIMO antenna must incorporate an efficient isolation mechanism. There are several ways to prevent mutual coupling in a MIMO system, including decoupling networks, defective ground structures, current localization, neutralization lines, integrating parasitic elements, antenna position and orientation, and others [125–130]. Incorporating MTM in the antenna design has proved an effective way to improve isolation. While acting as a decoupling mechanism between the neighbouring antenna elements, the use of MTM structure in the MIMO antenna affects the current distribution. The resonant behaviour of MTM structure prevents mutual coupling by containing the magnetic field inside the stimulated antenna.

3.3.1 MTM/MS loading on the main resonator

At 5.5 GHz, the surface current distribution is investigated to explain how the MS contributes to the suppression of surface waves, which reduces mutual coupling [83]. As shown in Fig. 27(a), antenna 1 is excited and a significant mutual coupling current occurs at the nearby antenna without MS. However, by introducing the MS as a backplane as in Fig. 27(b), the coupling current gets distributed to the unit cells of the MS and achieves isolation between multiple elements of the antenna. The arrangement delivers envelope correlation coefficient (ECC) < 0.004, diversity gain (DG) > 9.98 dB, and isolation > 15.5 dB with an efficiency of 82%.

Two elements of the MIMO antenna are arranged next to one another with a 0.135 λ_0 (7 mm) edge-to-edge spacing in Ref. 13 to be operated at 5.8 GHz. By retaining the MTM structure in between the MIMO parts, isolation is improved by 9 dB. In order to reduce the mutual coupling between two radiating elements, an MTM design is inserted between them as shown in Fig. 28(a). With this design, isolation is improved by 9 dB, ECC is < 0.1 dB, channel capacity loss (CCL) is < 0.05 bits/s/Hz and DG is > 9 dB. Figure 28(b) shows acceptable values of input port voltage reflection coefficient – $|S_{11}|$ and reverse voltage gain – $|S_{12}|$ parameters, which are highly desired for MIMO antennae.

(a)

(b)

(c)
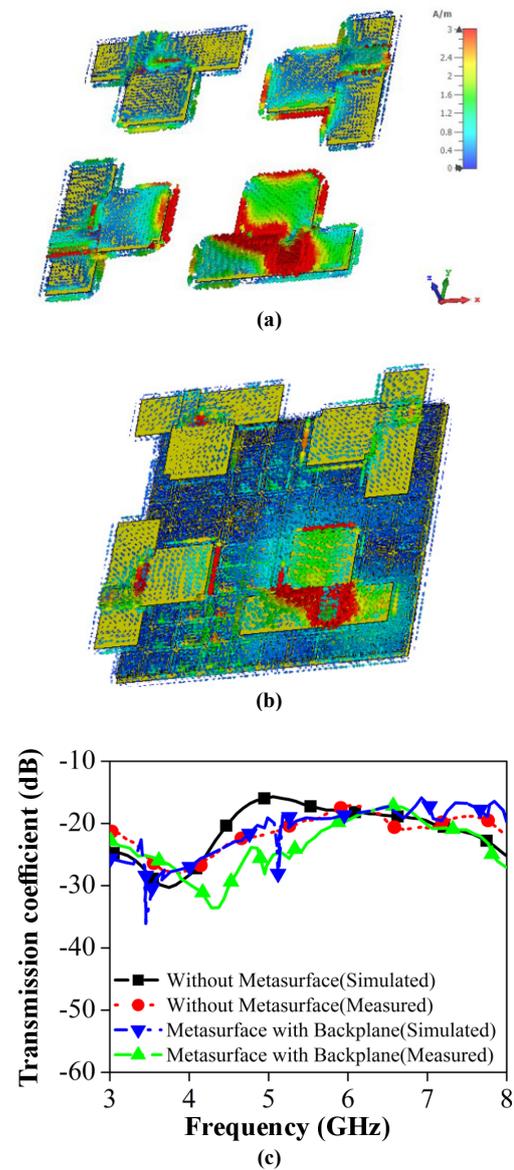
Fig. 27. MIMO antenna arrangement for isolation improvement (reproduced with permission [83]). (a) Surface current distribution without MS, (b) with MS as a back plane, (c) $|S_{12}|$ and $|S_{34}|$ plot.

Reference 132 describes the development of an improved isolation and gain of MIMO antenna based on MTMs. The superstrate is made of a novel hexagonal-shaped nested loop DNG MTM. It is mounted above the MIMO antenna and demonstrates isolation exceeding 24 dB over the full WLAN band (5.68–6.05 GHz) with a peak gain of 7.98 dBi. Two rectangular patch antennae of the same dimension (18 mm × 16 mm) are developed with coaxial probe feeding and printed on an RT/Duroid 5870 substrate with $\varepsilon_r = 2.33$. The superstrate has an arrangement of eight MTM cells in two rows separated by $d_1 = 10$ mm and the thickness of superstrate $H = 9$ mm, the mutual coupling brought on by near-field radiation was reduced because of the optimum values of d_1 and H. The simulated and measured $|S_{21}|$ plots of the implemented antenna are shown in Fig. 29.

The MIMO antenna can potentially use near-field resonators (NFR) to improve isolation between antenna elements. The distribution of surface current in antenna 1

(a)

(b)

(c)
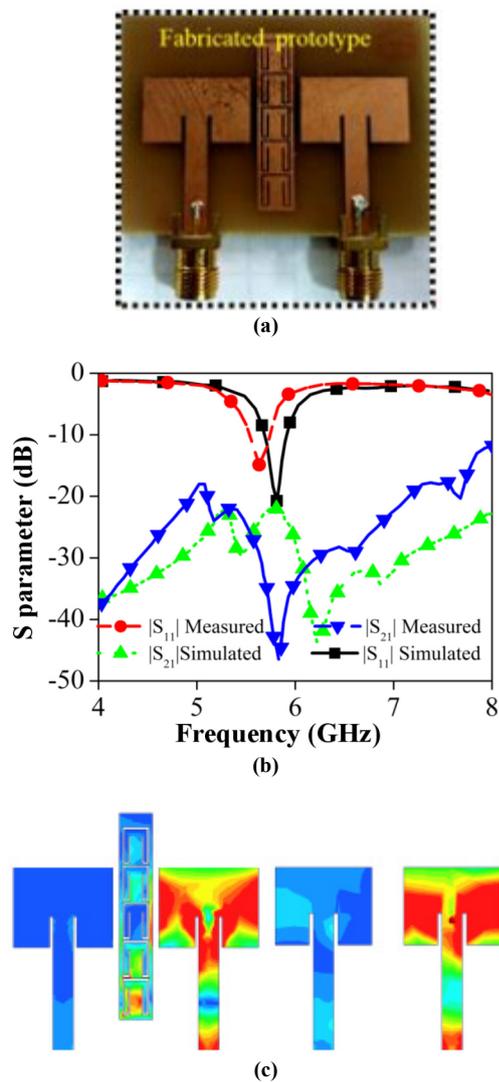
Fig. 28. MTM-based two-port MIMO antenna (reproduced with permission [131]). (a) Fabricated antenna, (b) S-parameters plot, (c) distribution of surface current in antenna patches with MTM (left) without MTM (right).
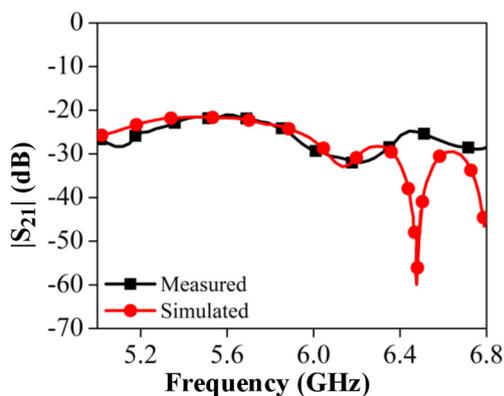
Fig. 29. $|S_{21}|$ plot.

is restricted to only antenna 1 by generating a perpendicular coupling mode at the operational resonant frequency in Ref. 133. NFRs are positioned above the radiating patch to provide isolation greater than 20 dB. The antenna substrate acts as a transmission medium. The connection between the patch and the air will generate a magnetic field encircling

it. The current distribution graphic shows that an antenna with no NFR has a substantial coupling between the antennae. NFR will consequently limit the magnetic field loops inside the stimulated antenna element by being placed atop the patch.

Incorporating MS in antenna design is an efficient way of minimizing mutual coupling. Reference 134 provides an illustration of the design architecture for the alumina-based dual-port dielectric resonators MIMO antenna. Two square-shaped apertures make up the top conducting part, and microstrip feed is employed on the substrate bottom side for excitation. Over the square-shaped aperture are two alumina-based dielectric resonators. On the two-port antennae, an MS layer made of a square unit cell with a diagonal cut made of FR-4 (0.8 mm thick) is hung at a height of 15 mm. This antenna design achieves a reduced mutual coupling value of −12 to −15 dB as in Fig. 30, ECC < 0.005, DG < 9.95 dB for a frequency band of 3.8 to 4.2 GHz.
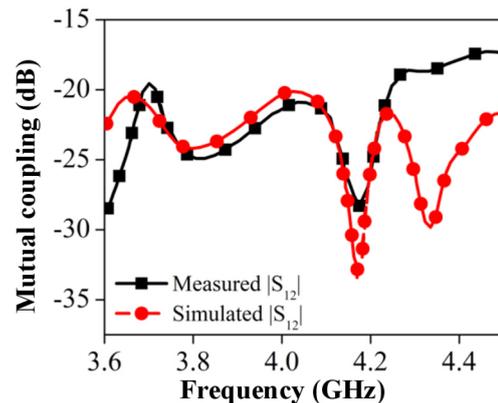
Fig. 30. Mutual coupling plot of MS-MIMO-DRA design.

An MS sheet with 8 × 8 square cell is placed on a 2 × 2 lower-end truncated rectangular patches [135]. Also, a decoupling structure comprised of slots and a metallic strip containing shorting pins are incorporated for enhanced isolation between antenna elements. This arrangement achieves isolation > 32 dB, ECC < 0.001, DG > 9.99 dB, and a peak gain of 8.72 dB.

3.3.2 MTM/MS inspired antenna

SRR and CSRR layouts are frequently used in the design of an antenna to improve isolation between elements of the MIMO antenna. In Ref. 136, a Vivaldi antenna equipped with the microstrip feeding line is suggested, and a triple-band gap CSRR is employed to decrease mutual coupling among the antenna parts. Concerning the band-stopping properties of the CSRR, the mutual coupling among the two Vivaldi antenna arrays and this structure is decreased. At 3.65, 4.9, and 5.8 GHz, the design improved decoupling by 8.5, 10.5, and 18 dB as shown in Fig. 31.

To prevent surface wave propagation, a unique slit-embedded mushroom EBG has been introduced between antenna elements [137]. Additionally, to improve the decoupling effect, CSRRs and H-shape defective ground structure (HDGS) have been deposited in the ground near antenna edges as shown in Fig. 32. This design achieves a 12 dB reduction in mutual coupling and an improved gain of 4.9 dBi at 3.25 GHz.
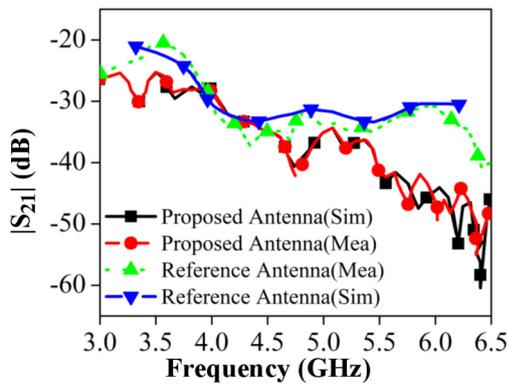
Fig. 31. S-parameters plot of Vivaldi antenna.

(a)

b)
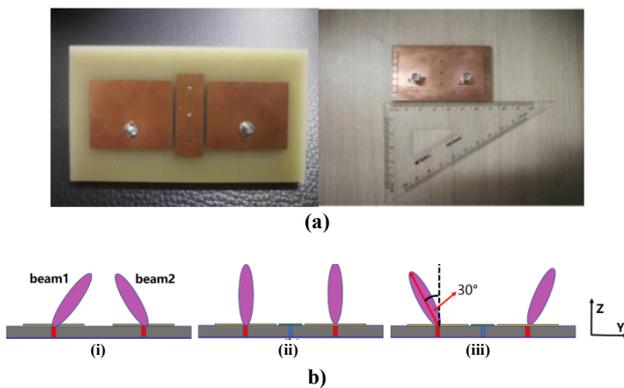
Fig. 32. EBG-CSRR-HDGS antenna design (reproduced with permission [137]). (a) Antenna prototype top view (left) and bottom view (right), (b) schematic of antenna beam states (i) without decoupling arrangement, (ii) EBG addition, (iii) EBG and CSRR addition.

Reference 138 has four antenna elements, out of which two are tuned for digital cellular system (DCS) downlink, and two are tuned for uplink at 2.45 GHz and 875 MHz, respectively. Two SRRs are placed between antenna elements, which achieves isolation of 17 dB, ECC < 0.0024 dB, DG > 9.9 dB, and CCL < 0.4 bits/s/Hz.

3.3.3 MTM/MS-integrated substrate

With the use of magnetic MTMs, isolation can be improved between the MIMO antenna elements by adjusting the near-field magnetic coupling among adjacent antennas. One can adjust the near-field magnetic coupling among antennae by tuning magnetic MTMs artificially created with negative or large permeability, which can absorb or block magnetic field lines where they are positioned. MTMs can improve antenna isolation in two different ways. The magnetic field lines can be pulled toward the edges of the antenna array using MTM with high permeability, or they can be prevented in spaces between neighbouring antennas. Reference 139 showed a four-element MIMO antenna with a substrate-integrated SRR (SI-SRR). On the one hand, the active antenna magnetic fields are prevented from slipping through the cracks into their neighbours, and on the other, they are directed in the direction of the bottom-left boundary corners. Magnetic couplings among array elements are reduced by the combination of blocking in gaps and guiding toward the
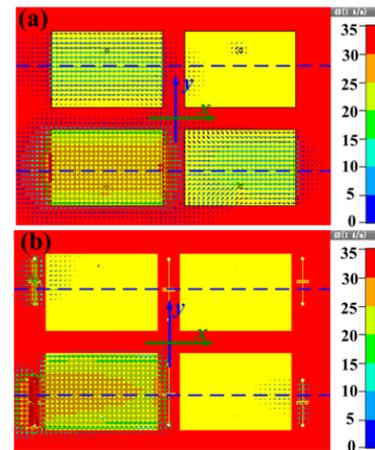
Fig. 33. H-field vector distribution of the densely packed patches on the surface of the antenna array at 3.5 GHz (reproduced with permission [139]). (a) Without integrated SI-SRRs and (b) with integrated SI-SRRs.

(a)   **(b)**

(c)
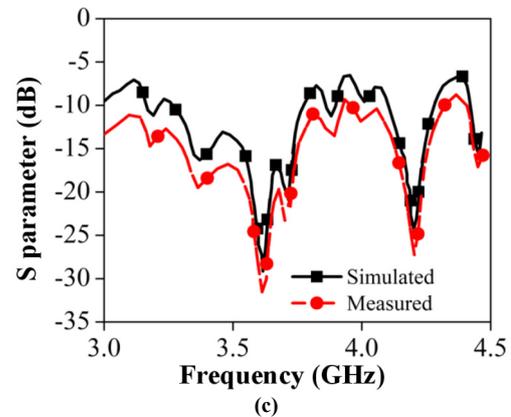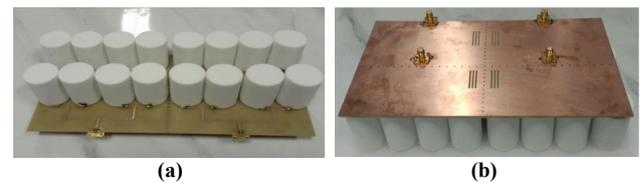
Fig. 34. Massive 4 × 4 MIMO antenna (reproduced with permission [140]). (a) Front view, (b) back view, (c) S-parameter plot.

borders as in Fig. 33. This arrangement provides better simulated and measured results.

In Ref. 140, the patch antenna will have a dielectric resonator on it, and an EBG structure will be added in between the elements of the MIMO antenna. Finally, the defective ground structure (DGS) should then be positioned on the ground plane. This arrangement is done for an 8 × 8 MIMO antenna array with an operating frequency of 3.4 GHz. Simulation results showed a reduction in mutual coupling of 15 dB, hence enhancing isolation, increased gain of 24.7 dB, increased bandwidth, and better ECC values. However, a 4 × 4 MIMO antenna was fabricated, which was assumed to represent a massive 8 × 8 antenna, as shown in Fig. 34. This 4 × 4 antenna showed similar results as that of the 8 × 8 comparison.

The summary of work on isolation enhancement is presented in Table 3.

Table 3.
Summary of work on isolation enhancement.

Ref.	MTM type	Isolation (dB)	ECC	DG (dB)	CCL	Gain (dB)	MIMO elements
[84]	CSRR cell MS	Improved by 5 dB	< 0.5	9.99	< 0.4	10.27	4
[131]	Rotated CSRR + Half-mode SIW + DGS	<−20 dB	0.4	> 9		4.3	2
[141]	ENG MTM	> 20	< 0.0025		< 0.35	7	8
[142]	Frequency selective surface + partially reflecting surface	> 20	< 0.11			7.2	4
[143]	SRR	> 20	0.001	10	0.358	6	2
[144]	EBG	> 15	0.015	9.95		7	2
[145]	CRLH	> 35	0.0002	10	–	–	2

4. Conclusions

The use of MTMs/MSs in the construction of microstrip patch antennae has shown to be a game-changing strategy, providing many advantages and improving antenna performance in multiple ways. Engineers and scientists have been able to bypass conventional constraints and achieve great breakthroughs in antenna technology by integrating MTM substrates or resonant elements. The historical development of EM MTMs has been emphasized in this review paper. By specifically examining the arrangement of MTM structures on or near the patch or the ground plane, substrate integration and superstrate layer with an air gap to the patch, the potential use of MTMs for antenna gain and bandwidth enhancement, improvement in isolation, and conversion from LC to CP has received more attention. In particular, i) MTM/MS loading on the main resonator with ENG, MNG material, high permittivity, and permeability cell, NRFP, CRLH techniques, and antenna design using EBG, DRA, usage of MS layer as superstrate or backplane were investigated. As well as, ii) MTM/MS inspired antenna using SRR and CSRR, and iii) MTM/MS integrated substrate. The reviewed results show that MTM/MS inclusion in the antenna design is a proven method to improve the important antenna parameters for high-end applications.

Abbreviations

CP – circular polarization
LP – linear polarization
LTE – long-term evolution
PCB – printed circuit board
MTM – metamaterial
EM – electromagnetic
MS – metasurface
ELC – electrics inductive capacitive
2D – two-dimensional
3D – three-dimensional
MIMO – multiple-input multiple-output
DoA – direction of arrival
EBG, EMBG – EM band gap
ENG – epsilon negative
MNG – μ-negative
SRR – split ring resonator
CSRR – complementary split ring resonator

DPS – double positive
DNG – double negative
CRLH – composite right/left-handed
LWA – leaky-wave antenna
DRA – dielectric resonator antenna
SIW – substrate integrated waveguide
RHCP – right hand cp
LHCP – left hand cp
AR – axial ratio
CSR – circular split ring
HIS – high impedance surface
CLL – capacitively-loaded loop
ECC – envelope correlation coefficient
CCL – channel capacity loss
DG – diversity gain
NFR – near-field resonators
DGS – defective ground structure
AMC – artificial magnetic conductor
PEC – perfect electric conductor
ZOR – zeroth order resonant
MNM – μ-negative MTM
PRS – partially reflecting surface
NFRP – near-field resonant parasitic
NLOS – non-line-of-sight
PTFE – polytetrafluoroethylene
HDGS – H-shape defective ground structure

References

[1]   Wang, C., Chen, Y. & Yang, S. Dual-band dual-polarized antenna array with flat-top and sharp cutoff radiation patterns for 2G/3G/LTE cellular bands. *IEEE Trans. Antennas Propag.* **66**, 5907–5917 (2018). https://doi.org/10.1109/TAP.2018.2866596

[2]   Yang, D., Liu, S. & Zhao, Z. A broadband dual-polarized printed dipole antenna with low cross-polarization and high isolation for base station applications. *Microw. Opt. Technol. Lett.* **59**, 1107–1111 (2017). https://doi.org/10.1002/mop.30467

[3]   Zheng, D.-Z. & Chu, Q.-X. A wideband dual-polarized antenna with two independently controllable resonant modes and its array for base-station applications. *IEEE Antennas Wirel. Propag. Lett.* **16**, 2014–2017 (2017). https://doi.org/10.1109/LAWP.2017.2693392

[4]   Tang, Z., Liu, J., Cai, Y.-M., Wang, J. & Yin, Y. A wideband differentially fed dual-polarized stacked patch antenna with tuned slot excitations. *IEEE Trans. Antennas Propag.* **66**, 2055–2060 (2018). https://doi.org/10.1109/TAP.2018.2800764

[5]   Huang, H., Li, X. & Liu, Y. A novel vector synthetic dipole antenna and its common aperture array. *IEEE Trans. Antennas Propag.* **66**, 3183–3188 (2018). https://doi.org/10.1109/TAP.2018.2819894

[6]   Ding, C., Sun, H.-H., Ziolkowski, R. W. & Jay Guo, Y. A dual layered loop array antenna for base stations with enhanced cross-polarization discrimination. *IEEE Trans. Antennas Propag.* **66**, 6975–6985 (2018). https://doi.org/10.1109/TAP.2018.2869216

[7]   Zhang, Q. & Gao, Y. A compact broadband dual-polarized antenna array for base stations. *IEEE Antennas Wirel. Propag. Lett.* **17**, 1073–1076 (2018). https://doi.org/10.1109/LAWP.2018.2832293

[8]   Ding, C. F, Zhang, X. Y, Zhang, Y., Mei Pan, Y. & Xue, Q. Compact broadband dual-polarized filtering dipole antenna with high selectivity for base-station applications. *IEEE Trans. Antennas Propag.* **66**, 5747–5756 (2018). https://doi.org/10.1109/TAP.2018.2862465

[9]   Liang, Z., Lu, C., Li, Y., Liu, J. & Long, Y. A broadband dual-polarized antenna with front-to-back ratio enhancement using semicylindrical sidewalls. *IEEE Trans. Antennas Propag.* **66**, 3735–3740 (2018). https://doi.org/10.1109/TAP.2018.2835500

[10]   EM Possible. *Advanced Electromagnetics: 21st Century Electro-magnetics (lecture online)*. https://empossible.net/wp-content/uploads/2020/06/Lecture-Intro-to-EM-Properties-of-Materials.pdf (2020).

[11]   *Metamaterials. Theory, design, and applications.* (eds. Cui, T. J, Smith, D. R. & Liu, R.) 1–367 (Springer, 2010). https://doi.org/10.1007/978-1-4419-0573-4

[12]   Bose, J. C. On the rotation of plane of polarisation of electric wave by a twisted structure. *Proc. R. Soc. London* **63**,146–152 (1898). https://doi.org/10.1098/rspl.1898.0019

[13]   Lindell, I. V., Sihvola, A. H. Kurkijarvi, J. Karl F. Lindman: the last Hertzian, and a harbinger of electromagnetic chirality. *IEEE Antennas Propag. Mag.* **34**, 24–30 (1992). https://doi.org/10.1109/74.153530

[14]   Kock, W. E. Metallic delay lenses. *Bell Syst. Tech. J.* **27**, 58–82 (1948). https://doi.org/10.1002/j.1538-7305.1948.tb01331.x

[15]   Engheta, N. Metamaterials with negative permittivity and permeability: background, salient features, and new trends. in *IEEE MTT-S International Microwave Symposium Digest* 187–190 (IEEE, 2003).

[16]   Veselago. V. G. (1968) The electrodynamics of substances with simultaneously negative values of ε and μ. *Sov. Phys. Usp.* **10**, 509–514 (1968). https://doi.org/10.1070/PU1968v010n04ABEH003699

[17]   Pendry, J. B., Holden, A. J, Stewart, W. J. & Youngs, I. Extremely low frequency plasmons in metallic mesostructures. *Phys. Rev. Lett.* **76**, 4773 (1996). https://doi.org/10.1103/PhysRevLett.76.4773

[18]   Pendry, J. B., Holden, A. J., Robbins, D. J., Stewart, W. J. Magnetism from conductors and enhanced nonlinear phenomena. *IEEE Trans. Microw. Theory Tech.* **47**, 2075–2084 (1999). https://doi.org/10.1109/22.798002

[19]   Smith, D. R., Padilla, W. J., Vier, D. C., Nemat-Nasser, S. C. & Schultz, S. Composite medium with simultaneously negative permeability and permittivity. *Phys. Rev. Lett.* **84**, 4184–4187 (2000). https://doi.org/10.1103/PhysRevLett.84.4184

[20]   Shelby, R. A., Smith, D. R. & Schultz, S. Experimental verification of a negative index of refraction. *Science* **292**,77–79 (2001). https://doi.org/10.1126/science.1058847

[21]   Nakano, H. *Low-Profile Natural and metamaterial Antennas.* (Wiley, 2016).

[22]   Esmail, B. A. F., Koziel, S. & Szczepanski, S. Overview of planar antenna loading MTMs for gain performance enhancement: The two decades of progress. *IEEE Access* **10**, 27381–27403 (2022). https://doi.org/10.1109/ACCESS.2022.3157634

[23]   Sydoruk, O., Tatartschuk, E., Shamonina, E. & Solymar, L. Analytical formulation for the resonant frequency of split rings. *J. Appl. Phys.* **105**, 014903 (2009). https://doi.org/10.1063/1.3056052

[24]   Vel Tech, *Final Year Project – Metamaterial Based Antenna* (2019). at https://www.youtube.com/watch?v=elbzxT_qxzc

[25]   Meta Group. Novel Electromagnetic Media. *Creating artificial response with metamaterials.* http://people.ee.duke.edu/~drsmith/metamaterials/metamaterial_elements.htm

[26]   Glybovski, S. B., Tretyakov, S. A., Belov, P. A., Kivshar, Y. S. & Simovski, C. R. Metasurfaces: from microwaves to visible. *Phys. Rep.* **634**, 1–72 (2016). https://doi.org/10.1016/j.physrep.2016.04.004

[27]   Walia, S. *et al.* Flexible metasurfaces and metamaterials: A review of materials and fabrication processes at micro- and nano-scales.

Appl. Phys. Rev. **2**, 011303 (2015). https://doi.org/10.1063/1.4913751

[28]   Chen, Z., Guo, B., Yang, Y. & Cheng, C. Metamaterials-based enhanced energy harvesting: A review. *Phys. B Condens. Matter.* **438**, 1–8 (2014). https://doi.org/10.1016/j.physb.2013.12.040

[29]   Syed Nasser, S. S., Liu, W. & Chen, Z. N. Wide bandwidth and enhanced gain of a low-profile dipole antenna achieved by integrated suspended metasurface. *IEEE Trans. Antennas Propag.* **66**, 1540–1544 (2018). https://doi.org/10.1109/TAP.2018.2790161

[30]   Sharawi, M. S. Printed multi-band MIMO antenna systems and their performance metrics [Wireless Corner]. *IEEE Antennas Propag. Mag.* **55**, 218–232 (2013). https://doi.org/10.1109/MAP.2013.6735522

[31]   Alibakhshikenari, M. *et al.* Interaction between closely packed array antenna elements using meta-surface for applications such as MIMO systems and synthetic aperture radars. *Radio Sci.* **53**, 1368–1381 (2018). https://doi.org/10.1029/2018RS006533

[32]   Alibakhshikenari, M. *et al.* A New Study to Suppress Mutual-Coupling Between Waveguide Slot Array Antennas Based on Metasurface Bulkhead for MIMO Systems. in *2018 Asia-Pacific Microwave Conference (APMC)* 500–502 (IEEE, 2018).

[33]   Alibakhshikenari, M. *et al.* Study on Antenna Mutual Coupling Suppression Using Integrated Metasurface Isolator for SAR and MIMO Applications. in *2018 48th European Microwave Conference (EuMC)* 1425–1428 (IEEE, 2018).

[34]   Alibakhshikenari, M. *et al.* Meta-surface wall suppression of mutual coupling between microstrip patch antenna arrays for THz-band applications. *Prog. Electromagn. Res. Lett.* **75**, 105–111 (2018). https://doi.org/10.2528/PIERL18021908

[35]   Lin, I.-H., DeVincentis, M., Caloz, C. & Itoh, T. Arbitrary dual-band components using composite right/left-handed transmission lines. *IEEE Trans. Microw. Theory Tech.* **52**, 1142–1149 (2004). https://doi.org/10.1109/TMTT.2004.825747

[36]   Thomas, Z. M., Grzegorczyk, T. M., Wu, B.-I., Chen. X. & Kong, J. A. Design and measurement of a four-port device using metamaterials. *Opt. Express* **13**, 4737–4744 (2005). https://doi.org/10.1364/OPEX.13.004737

[37]   Caloz, C. & Itoh, T. A novel mixed conventional microstrip and composite right/left-handed backward-wave directional coupler with broadband and tight coupling characteristics. *IEEE Microw. Wirel. Compon. Lett.* **14**, 31–33 (2004). https://doi.org/10.1109/LMWC.2003.821506

[38]   Antoniades, M. A. & Eleftheriades, G. V. A broadband Wilkinson balun using microstrip metamaterial lines. *IEEE Antennas Wirel. Propag. Lett.* **4**, 209–212 (2005). https://doi.org/10.1109/LAWP.2005.851005

[39]   Abbasi, M. A. B., Antoniades, M. A. & Nikolaou, S. A compact reconfigurable NRI-TL MTM phase shifter for antenna applications. *IEEE Trans Antennas Propag.* **66**, 1025–1030 (2018). https://doi.org/10.1109/TAP.2017.2777520

[40]   Cao, T., Wei, C., Simpson, R. E., Zhang, L. & Cryan, M. J. Broadband polarization-independent perfect absorber using a phase-change metamaterial at visible frequencies. *Sci. Rep.* **4**, 3955 (2014). https://doi.org/10.1038/srep03955

[41]   Thomas, Z. M., Grzegorczyk, T. M., Wu, B.-I. & Kong, J. A. Enhanced microstrip stopband filter using a metamaterial substrate. *Microw. Opt. Technol. Lett.* **48**, 1522–1525 (2006). https://doi.org/10.1002/mop.21703

[42]   Zvolensky, T., Gollub, J. N., Marks, D. L. & Smith, D. R. Design and analysis of a W-band metasurface-based computational imaging system. *IEEE Access* **5**, 9911–9918 (2017). https://doi.org/10.1109/ACCESS.2017.2703860

[43]   Modi, A. Y., Balanis, C. A., Birtcher, C. R. & Shaman, H. New class of RCS-reduction metasurfaces based on scattering cancellation using array theory. *IEEE Trans. Antennas Propag.* **67**, 298–308 (2019). https://doi.org/10.1109/TAP.2018.2878641

[44]   Faruque, M. R. I., Ahamed, E., Rahman, M. A. & Islam, M. T. Flexible nickel aluminate (NiAl2O4) based dual-band double negative metamaterial for microwave applications. *Results Phys.* **14**, 102524 (2019). https://doi.org/10.1016/j.rinp.2019.102524

[45]   Ramachandran, T., Faruque, M. R. I & Ahamed, E. Composite circular split ring resonator (CSRR)-based left-handed metamaterial for C- and Ku-band application. *Results Phys.* **14**, 102435 (2019). https://doi.org/10.1016/j.rinp.2019.102435

[46] Chuma, E. L., Iano, Y., Fontgalland, G. & Bravo Roger, L. L. Microwave sensor for liquid dielectric characterization based on metamaterial complementary split ring resonator. *IEEE Sens. J.* **18**, 9978–9983 (2018). https://doi.org/10.1109/JSEN.2018.2872859

[47] Chen, H. *et al*. Magnetic properties of s-shaped split-ring resonators. *Prog. Electromagn. Res.* **51**, 231–247 (2005). https://doi.org/10.2528/PIER04051201

[48] Greegor, R. B. *et al*. Simulation and testing of a graded negative index of refraction lens. *Appl. Phys. Lett.* **87**, 091114 (2005). https://doi.org/10.1063/1.2037202

[49] Smith, D. L., Medgyesi-Mitschang, L. N. & Forester, D. W. Surface integral equation formulations for left-handed materials. *Prog. Electromagn. Res.* **51**, 27–48 (2005). https://doi.org/10.2528/PIER04032203

[50] Zeng, Y. *et al*. A Matryoshka-like seismic metamaterial with wide band-gap characteristics. *Int. J. Solids Struct.* **185–186,** 334–341 (2020). https://doi.org/10.1016/j.ijsolstr.2019.08.032

[51] Abielmona. S., Nguyen, H. V. & Caloz, C. Analog direction of arrival estimation using an electronically-scanned CRLH leaky-wave antenna. *IEEE Trans. Antennas Propag.* **59**, 1408–1412 (2011). https://doi.org/10.1109/TAP.2011.2109672

[52] Lim, S., Caloz, C. & Itoh, T. Metamaterial-based electronically controlled transmission-line structure as a novel leaky-wave antenna with tunable radiation angle and beamwidth. *IEEE Trans. Microw. Theory Tech.* **52**, 2678–2690 (2004). https://doi.org/10.1109/TMTT.2004.838302

[53] Alibakhshikenari, M. *et al*. Mutual-coupling isolation using embedded metamterial EM bandgap decoupling slab for densely packed array antennas. *IEEE Access* **7**, 51827–51840 (2019). https://doi.org/10.1109/ACCESS.2019.2909950

[54] Alibakhshikenari, M. *et al*. Mutual coupling suppression between two closely placed microstrip patches using em-bandgap MTM fractal loading. *IEEE Access* **7**, 23606–23614 (2019). https://doi.org/10.1109/ACCESS.2019.2899326

[55] Alibakhshikenari, M., Virdee, B. S., Ali, A. & Limiti, E. A novel monofilar-Archimedean MTM inspired leaky-wave antenna for scanning application for passive radar systems. *Microw. Opt. Technol. Lett.* **60**, 2055–2060 (2018). https://doi.org/10.1002/mop.31300

[56] Caloz, C., Itoh, T. & Rennings, A. CRLH metamaterial leaky-wave and resonant antennas. *IEEE Antennas Propag. Mag.* **50**, 25–39 (2008). https://doi.org/10.1109/MAP.2008.4674709

[57] Antoniades, M. A., Zhu, J., Selvanayagam, M. & Eleftheriades, G. V. Compact, Wideband and Multiband Antennas Based on Metamaterial Concepts. in *Proceedings of the Fourth European Conference on Antennas and Propagation* 1–5 (IEEE, 2010).

[58] Alibakhshikenari, M. *et al*. Beam-scanning leaky-wave antenna based on CRLH-MTM for millimetre-wave applications. *IET Microw. Antennas Propag.* **13**, 1129–1133 (2019). https://doi.org/10.1049/iet-map.2018.5101

[59] Bongard, F. & Mosig, J. R. A Novel Composite Right/Left-Handed Unit Cell and Potential Antenna Applications. in *2008 IEEE Antennas and Propagation Society International Symposium* 1–4 (IEEE, 2008).

[60] Liu, L., Caloz, C. & Itoh, T. Dominant mode leaky-wave antenna with backfire-to-endfire scanning capability. *Electron. Lett.* **38**, 1414–1416 (2002). https://doi.org/10.1049/el:20020977

[61] Dash, U. A. & Sahu, S. Gain enhancement of truncated conical dielectric ring resonator antenna based on metasurface walls. *Int. J. RF Microw. Comput. Eng.* **28**, e21499 (2018). https://doi.org/10.1002/mmce.21499

[62] Erentok, A. & Ziolkowski, R. W. Metamaterial-inspired efficient electrically small antennas. *IEEE Trans. Antennas Propag.* **56**, 691–707 (2008). https://doi.org/10.1109/TAP.2008.916949

[63] Venkateswara Rao, M., Madhav, B. T. P., Anilkumar, T. & Prudhvi Nadh, B. Metamaterial-inspired quad band circularly polarized antenna for WLAN/ISM/Bluetooth/WiMAX and satellite communication applications. *AEU – Int. J. Electron. Commun.* **97**, 229–241 (2018). https://doi.org/10.1016/j.aeue.2018.10.018

[64] Panda, A. K., Sahu, S. & Mishra, R. K. DRA gain enhancement using a planar metamaterial superstrate. *Int. J. RF Microw. Comput. Eng.* **28**, e21445 (2018). https://doi.org/10.1002/mmce.21445

[65] Alibakhshikenari, M. *et al*. High-isolation leaky-wave array antenna based on CRLH-MTM implemented on SIW with ±30º

frequency beam-scanning capability at millimetre-waves. *Electronics* **8**, 642 (2019). https://doi.org/10.3390/electronics8060642

[66] Sihvola, A., Semchenko, I. & Khakhomov, S. View on the history of electromagnetics of metamterials: Evolution of the congress series of complex media. *Photonics Nanostructures – Fundam. Appl.* **12**, 279–283 (2014). https://doi.org/10.1016/j.photonics.2014.03.004

[67] Li, A., Singh, S. & Sievenpiper, D. Metasurfaces and their applications. *Nanophotonics* **7**, 989–1011 (2018). https://doi.org/10.1515/nanoph-2017-0120

[68] Zheng, Y. *et al*. Metamaterial-based patch antenna with wideband RCS reduction and gain enhancement using improved loading method. *IET Microw. Antennas Propag.* **11**, 1183–1189 (2017). https://doi.org/10.1049/iet-map.2016.0746

[69] Nabil, M. & Faisal, M. M. A. Design, Simulation and analysis of a high gain small size array antenna for 5G wireless communication. *Wirel. Pers. Commun.* **116**, 2761–2776 (2021). https://doi.org/10.1007/s11277-020-07819-9

[70] Augustin, G., Rao, Q. & Denidni, T. A. Low-Profile Antennas. in *Handbook of Antenna Technologies (eds:Chen, Z.-N., Liu, D., Nakana, H., Qing, X. & Zwick, T.)* 1531–1564 (Springer, 2016).

[71] Nasimuddin & Esselle, K. P, A low-profile compact microwave antenna with high gain and wide bandwidth. *IEEE Trans. Antennas Propag.* **55**, 1880–1883 (2007). https://doi.org/10.1109/TAP.2007.898644

[72] Wang, Z. & Liu, J. A compact directional microstrip antenna with wide bandwidth, high gain, and high front-to-back ratio. *Microw. Opt. Technol. Lett.* **62**, 308–314 (2020). https://doi.org/10.1002/mop.32007

[73] Wang, J., Liu, Q. & Zhu, L. Bandwidth enhancement of a differential-fed equilateral triangular patch antenna via loading of shorting posts. *IEEE Trans. Antennas Propag.* **65**, 36–43 (2017). https://doi.org/10.1109/TAP.2016.2630660

[74] Katyal, A. & Basu, A. Compact and broadband stacked microstrip patch antenna for target scanning applications. *IEEE Antennas Wirel. Propag. Lett.* **16**, 381–384 (2017). https://doi.org/10.1109/LAWP.2016.2578723

[75] Xu, K. D., Xu, H., Liu, Y., Li, Y. & Liu, Q. H. Microstrip patch antennas with multiple parasitic patches and shorting vias for bandwidth enhancement. *IEEE Access* **6**, 11624–11633 (2018). https://doi.org/10.1109/ACCESS.2018.2794962

[76] Mandal, K. & Sarkar, P. P. A compact low profile wideband U-shape antenna with slotted circular ground plane. *AEU – Int. J. Electron. Commun.* **70**, 336–340 (2016). https://doi.org/10.1016/j.aeue.2015.12.011

[77] Alibakhshi-Kenari, M., Naser-Moghadasi, M., Sadeghzadeh, R. A., Virdee, B. S. & Lomiti, E. Bandwidth extension of planar antennas using embedded slits for reliable multiband RF communications. *AEU – Int. J. Electron. Commun.* **70**, 910–919 (2016). https://doi.org/10.1016/j.aeue.2016.04.003

[78] Roy, S. & Chakraborty, U. Metamaterial-embedded dual wideband microstrip antenna for 2.4 GHz WLAN and 8.2 GHz ITU band applications. *Waves Random Complex Media* **30**, 193–207 (2020). https://doi.org/10.1080/17455030.2018.1494396

[79] Roy, S. & Chakraborty, U. Gain enhancement of a dual-band WLAN microstrip antenna loaded with diagonal pattern metamaterials. *IET Commun.* **12**, 1448–1453 (2018). https://doi.org/10.1049/iet-com.2018.0170

[80] Sahoo, R. & Vakula, D. Gain enhancement of conformal wideband antenna with parasitic elements and low index metamaterial for WiMAX application. *AEU – Int. J. Electron. Commun.* **105**, 24–35 (2019). https://doi.org/10.1016/j.aeue.2019.03.014

[81] Urul, B. Gain enhancement of microstrip antenna with a novel DNG material. *Microw. Opt. Technol. Lett.* **62**, 1824–1829 (2020). https://doi.org/10.1002/mop.32240

[82] Ziolkowski, R. W. & Kipple, A. D. Application of double negative materials to increase the power radiated by electrically small antennas. *IEEE Trans. Antennas Propag.* **51**, 2626–2640 (2003). https://doi.org/10.1109/TAP.2003.817561

[83] Hasan, M. M. *et al*. Gain and isolation enhancement of a wideband MIMO antenna using metasurface for 5G sub-6 GHz communication systems. *Sci. Rep.* **12**, 9433 (2022). https://doi.org/10.1038/s41598-022-13522-5

[84] Tariq, S., Naqvi, S. I., Hussain, N. & Amin, Y. A metasurface-based MIMO antenna for 5G millimeter-wave applications. *IEEE Access* **9**, 51805–51817 (2021). https://doi.org/10.1109/ACCESS.2021.3069185

[85] Wang, J., Wong, H., Ji, Z. & Wu, Y. Broadband CPW-Fed aperture coupled metasurface antenna. *IEEE Antennas Wirel. Propag. Lett.* **18**, 517–520 (2019). https://doi.org/10.1109/LAWP.2019.2895618

[86] Panda, P. K. & Ghosh, D. Wideband and high gain tuning fork shaped monopole antenna using high impedance surface. *AEU – Int. J. Electron. Commun.* **111**, 152920 (2019). https://doi.org/10.1016/j.aeue.2019.152920

[87] Zheng, Y. *et al*. Wideband gain enhancement and RCS reduction of Fabry–Perot resonator antenna with chessboard arranged metamaterial superstrate. *IEEE Trans. Antennas Propag.* **66**, 590–599 (2018). https://doi.org/10.1109/TAP.2017.2780896

[88] Zhu, J., Li, S., Liao, S. & Xue, Q. Wideband low-profile highly isolated MIMO antenna with artificial magnetic conductor. *IEEE Antennas Wirel. Propag. Lett.* **17**, 458–462 (2018). https://doi.org/10.1109/LAWP.2018.2795018

[89] Pandeeswari, R. & Raghavan, S, Microstrip antenna with complementary split ring resonator loaded ground plane for gain enhancement. *Microw. Opt. Technol. Lett.* **57**, 292–296 (2015). https://doi.org/10.1002/mop.28835

[90] Ghosh, A., Mandal, T. & Das, S. Design of triple band slot-patch antenna with improved gain using triple band artificial magnetic conductor. *Radioengineering* **25**, 442–448 (2016). https://doi.org/10.13164/re.2016.0442

[91] Patel, S. K. & Argyropoulos, C. Enhanced bandwidth and gain of compact microstrip antennas loaded with multiple corrugated split ring resonators. *J. Electromagn. Waves Appl.* **30**, 945–961 (2016). https://doi.org/10.1080/09205071.2016.1167633

[92] Ikonen, P. M. T., Maslovski, S. I., Simovski, C. R. & Tretyakov, S. A. On artificial magnetodielectric loading for improving the impedance bandwidth properties of microstrip antennas. *IEEE Trans. Antennas Propag.* **54**, 1654–1662 (2006). https://doi.org/10.1109/TAP.2006.875912

[93] Cao, W., Ma, W., Peng, W. & Chen, Z. N. Bandwidth-enhanced electrically large microstrip antenna loaded with SRR structures. *IEEE Antennas Wirel. Propag. Lett.* **18**, 576–580 (2019). https://doi.org/10.1109/LAWP.2019.2896384

[94] Liu, Z., Wang, P. & Zeng, Z. Enhancement of the gain for microstrip antennas using negative permeability metamaterial on low temperature co-fired ceramic (LTCC) substrate. *IEEE Antennas Wirel. Propag. Lett.* **12**, 429–432 (2013). https://doi.org/10.1109/LAWP.2013.2254697

[95] Rahmat-Samii, Y. Electromagnetic Band Gap (EBG) Structures in Antenna Engineering: from Fundamentals to Recent Advances. in *2008 Asia-Pacific Microwave Conference* 1–2 (IEEE, 2008).

[96] Sambandam, P. *et al*. Compact monopole antenna backed with fork-slotted EBG for wearable applications. *IEEE Antennas Wirel. Propag. Lett.* **19**, 228–232 (2020). https://doi.org/10.1109/LAWP.2019.2955706

[97] Ahdi Rezaeieh, S., Antoniades, M. A. & Abbosh, A. M. Bandwidth and directivity enhancement of loop antenna by nonperiodic distribution of mu-negative metamaterial unit cells. *IEEE Trans. Antennas Propag.* **64**, 3319–3329 (2016). https://doi.org/10.1109/TAP.2016.2574878

[98] Arora, C., Pattnaik, S. S. & Baral, R. N. Performance enhancement of patch antenna array for 5.8 GHz Wi-MAX applications using MTM inspired technique. *AEU – Int. J. Electron. Commun.* **79**, 124–131 (2017). https://doi.org/10.1016/j.aeue.2017.05.045

[99] Meriche, M. A., Attia, H., Messai, A.,Mitu, S. S. I. & Denidni, T. A. Directive wideband cavity antenna with single-layer meta-superstrate. *IEEE Antennas Wirel. Propag. Lett.* **18**, 1771–1774 (2019). https://doi.org/10.1109/LAWP.2019.2929579

[100] Verma, A., Singh, A. K., Srivastava, N., Patil, S. & Kanaujia, B. K. Hexagonal ring electromagnetic band gap-based slot antenna for CP and performance enhancement. *Microw. Opt. Technol. Lett.* **62**, 2576–2587 (2020). https://doi.org/10.1002/mop.32342

[101] Chopra, R. & Kumar, G. Compact, broadband, and high gain directional endfire antenna. *Microw. Opt. Technol. Lett.* **62**, 2546–2553 (2020). https://doi.org/10.1002/mop.32336

[102] Wu, T., Chen, J. & Wu, P.-F. Broadband and multi-mode Fabry–Pérot cavity antenna with gain enhancement. *AEU – Int. J. Electron.*

Commun. **127**, 153440 (2020). https://doi.org/10.1016/j.aeue.2020.153440

[103] Sonak, R., Ameen, M. & Chaudhary, R. K. High gain dual-band open-ended MTM antenna utilizing CRR with broadside radiation characteristics based on left-handed AMC and PEC. *Mater. Res. Express* **6**, 055811 (2019). https://doi.org/10.1088/2053-1591/ab0683

[104] Kumar, S. & Kumari, R. Bandwidth enhanced coplanar waveguide-fed composite right/left handed antenna loaded with resonating rings. *IET Microw. Antennas Propag.* **13**, 2134–2140 (2019). https://doi.org/10.1049/iet-map.2018.5931

[105] Wong, K. *Compact and Broadband Microstrip Antennas.* (Wiley, 2002).

[106] Gao, S., Luo, Q. & Zhu, F. *Circularly Polarized Antennas.* (Wiley, 2014).

[107] Lee, S. W. & Sung, Y. J. Simple polarization-reconfigurable antenna with t-shaped feed. *IEEE Antennas Wirel. Propag. Lett.* **15**, 114–117 (2016). https://doi.org/10.1109/LAWP.2015.2432462

[108] Lin, W. & Wong, H. Wideband CP reconfigurable antenna. *IEEE Trans. Antennas Propag.* **63**, 5938–5944 (2015). https://doi.org/10.1109/TAP.2015.2489210

[109] Wang, K. X. & Wong, H. A reconfigurable CP/LP antenna with cross-probe feed. *IEEE Antennas Wirel. Propag. Lett.* **16**, 669–672 (2017). https://doi.org/10.1109/LAWP.2016.2598248

[110] Zhang, L., Gao, S., Luo, Q., Young, P. R. & Li, Q. Wideband loop antenna with electronically switchable CP. *IEEE Antennas Wirel. Propag. Lett.* **16**, 242–245 (2017). https://doi.org/10.1109/LAWP.2016.2570859

[111] Malathong, M., Sonsilphong, A., Panpradit, W. & Wongkasem, N. Chiral Metamatrisl Based Circularly Polarized Microstrip Antennas. in *2011 IEEE-APS Topical Conference on Antennas and Propagation in Wireless Communications* 898–901 (IEEE, 2011).

[112] Wang, W. *et al*. Subwavelength-cavity high-gain circularly polarized antenna with planar metamaterials. *Appl. Sci.* **13**, 7665 (2023). https://doi.org/10.3390/app13137665

[113] Tang, M.-C. & Ziolkowski, R. W. Frequency-agile, efficient, circularly polarized, near-field resonant antenna: Designs and measurements. *IEEE Trans Antennas Propag.* **63**, 5203–5209 (2015). https://doi.org/10.1109/TAP.2015.2477563

[114] Jin, P. & Ziolkowski, R. W. Multi-frequency, linear and circular polarized, metamaterial-inspired, near-field resonant parasitic antennas. *IEEE Trans. Antennas Propag.* **59**, 1446–1459 (2011). https://doi.org/10.1109/TAP.2011.2123053

[115] Chaudhary, P., Kumar, A., Kumar, P., Kanaujia, B. K. & Birwal, A. Design of a new metasurface and its application for linear to circular polarisation conversion. *Int. J. Electron.* **108**, 411–425 (2021). https://doi.org/10.1080/00207217.2020.1794050

[116] Zhu, H. L., Cheung, S. W., Chung, K. L. & Yuk, T. I. Linear-to-CP conversion using metasurface. *IEEE Trans. Antennas Propag.* **61**, 4615–4623 (2013). https://doi.org/10.1109/TAP.2013.2267712

[117] Goswami, S. & Karia, D. C. A metamaterial-inspired circularly polarized antenna for implantable applications. *Eng. Rep.* **2**, e12251 (2020). https://doi.org/10.1002/eng2.12251

[118] Arora, C. Metamaterial-Inspired Circularly Polarized Microstrip Patch Antenna. in *Computer Communication, Networking and IoT (eds. Bhateja, V., Satapathy, S. C., Traviezo-Gonzales, C. M. & Flores-Fuentes, V.)* 183–190 (Springer, 2021).

[119] Ashish, J. & Prakasa Rao, A. A dual band CRLH metamaterial-inspired planar antenna for wireless applications. *Radioengineering* **31**, 15–22 (2022). https://doi.org/10.13164/re.2022.0015

[120] Majeed, A. *et al*. An ultra-wideband linear-to-CP converter based on a circular, pie-shaped reflective metasurface. *Electronics* **11**, 1681 (2022). https://doi.org/10.3390/electronics11111681

[121] Montalvão, E. S. R., Montalvão, A. C. P. S., Campos, A. L. P. S. & Gomes Neto, A. A new model of metasurface used for linear-to-CP conversion in antenna array. *Microw. Opt. Technol. Lett.* **58**, 861–864 (2016). https://doi.org/10.1002/mop.29681

[122] Revathi, S., Sivakumar, E. & Ramachandran, B. Metasurface based circularly polarized reconfigurable antenna. *Indian J. Sci. Technol.* **9**, 1–8 (2016). https://doi.org/10.17485/ijst/2016/v9i44/101959

[123] Huang, Y., Yang, L., Li, J., Wang, Y. & Wen, G. Polarization conversion of metasurface for the application of wide band low-

profile CP slot antenna. *Appl. Phys. Lett.* **109**, 054101 (2016). https://doi.org/10.1063/1.4960198

[124] Chen, X., Zhang, S. & Li, Q. A review of mutual coupling in MIMO systems. *IEEE Access* **6**, 24706–24719 (2018). https://doi.org/10.1109/ACCESS.2018.2830653

[125] Liu, R. *et al*. Neutralization line decoupling tri-band multiple-input multiple-output antenna design. *IEEE Access* **8**, 27018–27026 (2020). https://doi.org/10.1109/ACCESS.2020.2971038

[126] Wang, L. *et al.* Compact UWB MIMO antenna with high isolation using fence-type decoupling structure. *IEEE Antennas Wirel. Propag. Lett.* **18**, 1641–1645 (2019). https://doi.org/10.1109/LAWP.2019.2925857

[127] Srivastava, G. & Mohan, A. Compact MIMO slot antenna for UWB applications. *IEEE Antennas Wirel. Propag. Lett.* **15**, 1057–1060 (2016). https://doi.org/10.1109/LAWP.2015.2491968

[128] Banerjee, J., Karmakar, A., Ghatak, R. & Poddar, D. R. Compact CPW-fed UWB MIMO antenna with a novel modified Minkowski fractal defected ground structure (DGS) for high isolation and triple band-notch characteristic. *J. Electromagn. Waves Appl.* **31**, 1550–1565 (2017). https://doi.org/10.1080/09205071.2017.1354727

[129] Wu, L., Xia, Y., Cao, X. & Xu, Z. A miniaturized UWB-MIMO antenna with quadruple band-notched characteristics. *Int. J. Microw. Wirel. Technol.* **10**, 948–955 (2018). https://doi.org/10.1017/S1759078718000508

[130] Hassan, M. M. *et al.* A novel UWB MIMO antenna array with band notch characteristics using parasitic decoupler. *J. Electromagn. Waves Appl.* **34**, 1225–1238 (2020). https://doi.org/10.1080/09205071.2019.1682063

[131] Iqbal, A., Saraereh, O. A., Bouazizi, A. & Basir, A. Metamaterial-based highly isolated MIMO antenna for portable wireless applications. *Electronics* **7**, 267 (2018). https://doi.org/10.3390/electronics7100267

[132] Mark, R., Rajak, N., Mandal, K. & Das, S. Metamaterial based superstrate towards the isolation and gain enhancement of MIMO antenna for WLAN application. *AEU – Int. J. Electron. Commun.* **100**, 144–152 (2019). https://doi.org/10.1016/j.aeue.2019.01.011

[133] Li, M., Zhong, B. G. & Cheung, S. W. Isolation enhancement for MIMO *patch antennas using near-field resonators as coupling-mode transducers. IEEE Trans. Antennas Propag.* **67**, 755–764 (2019). https://doi.org/10.1109/TAP.2018.2880048

[134] Dwivedi, A. K., Sharma, A., Singh, A. K. & Singh, V. Metamaterial inspired dielectric resonator MIMO antenna for isolation enhancement and linear to CP of waves. *Measurement* **182**, 109681 (2021). https://doi.org/10.1016/j.measurement.2021.109681

[135] Sufian, M. A. *et al*. Isolation enhancement of a metasurface-based MIMO antenna using slots and shorting pins. *IEEE Access* **9**, 73533–73543 (2021). https://doi.org/10.1109/ACCESS.2021.3079965

[136] Najafy, V. & Bemani, M. Mutual-coupling reduction in triple-band MIMO antennas for WLAN using CSRRs. *Int. J. Microw. Wirel. Technol.* **12**, 762–768 (2020). https://doi.org/10.1017/S1759078720000215

[137] Yang, Z., Xiao, J. & Ye, Q. Enhancing MIMO antenna isolation characteristic by manipulating the propagation of surface wave. *IEEE Access* **8**, 115572–115581 (2020). https://doi.org/10.1109/ACCESS.2020.3004467

[138] Kumar, A., Ansari, A. Q., Kanaujia, B. K. & Kishor, J. High isolation compact four-port MIMO antenna loaded with CSRR for multiband applications. *Frequenz* **72**, 415–427 (2018). https://doi.org/10.1515/freq-2017-0276

[139] Liu, Z. *et al.* Enhancing isolation of antenna arrays by simultaneously blocking and guiding magnetic field lines using magnetic metamaterials. *Appl. Phys. Lett.* **109**, 153505 (2016). https://doi.org/10.1063/1.4964513

[140] Sandi, E., Diamah, A. & Al Mawaddah, M. High isolation MIMO antenna for 5G C-band application by using combination of dielectric resonator, electromagnetic bandgap, and defected ground structure. *EURASIP J. Wirel. Commun. Netw.* **2022**, 125 (2022). https://doi.org/10.1186/s13638-022-02208-1

[141] Shabbir, T. *et al.* Eight-port metamaterial loaded UWB-MIMO antenna system for 3D system-in-package applications. *IEEE Access* **8**, 106982–106992 (2020). https://doi.org/10.1109/ACCESS.2020.3000134

[142] Das, G., Sahu, N. K., Sharma, A., Gangwar, R. K. & Sharawi, M. S. FSS-based spatially decoupled back-to-back four-port MIMO DRA with multidirectional pattern diversity. *IEEE Antennas Wirel. Propag. Lett.* **18**, 1552–1556 (2019). https://doi.org/10.1109/LAWP.2019.2922276

[143] Irene, G. & Rajesh, A. A dual-polarized UWB–MIMO antenna with IEEE 802.11ac band-notched characteristics using split-ring resonator. *J. Comput. Electron.* **17**, 1090–1098 (2018). https://doi.org/10.1007/s10825-018-1213-x

[144] Thakur, E., Jaglan, N. & Gupta, S. D. Design of compact triple band-notched UWB MIMO antenna with TVC-EBG structure. *J. Electromagn. Waves Appl.* **34,** 1601–1615 (2020). https://doi.org/10.1080/09205071.2020.1775136

[145] Ibrahim, A. A. & Abdalla, M. A. CRLH MIMO antenna with reversal configuration. *AEU – Int. J. Electron. Commun.* **70**, 1134–1141 (2016). https://doi.org/10.1016/j.aeue.2016.05.012